# Electromagnetic Scattering and Absorption by Thin Walled Dielectric Cylinders with Application to Ice Crystals

Thomas B.A. Senior and Herschel Weil

RL-632 = RL-632

The authors are with the University of Michigan, Department of Electrical and Computer Engineering Radiation Laboratory, Ann Arbor, Michigan 48109. Dr. Weil is presently on leave at the National Center for Atmospheric Research, Boulder, Colorado 80307.

## Abstract

Integral equations are developed to determine the scattering and absorption of electromagnetic radiation by thin walled cylinders of arbitrary cross-section and refractive index. Numerical data are presented at wavelengths in the infrared for hollow, circular and hexagonal cross-section cylinders which simulate columnar sheath ice crystals. The numerical procedures are economical for cylinders whose perimeters are less than about 15 free-space wavelengths.

## 1. Introduction

The reflection, transmission and absorption of visible and infrared radiation by clouds and by polluted atmospheres are of considerable practical importance. Cirrus clouds, in particular, are found all over the globe and have a profound effect on the atmospheric heat balance. The ice crystals which compose them scatter and absorb the predominantly ir radiation emanating from the earth and the lower regions of the atmosphere, as well as the mainly shorter wavelength solar radiation incident from above. The difference in the scattering and absorption properties of ice crystals in these two wavelength regions play a major part in the atmospheric heat balance which governs the global location of energy sources and sinks and, hence, the atmospheric circulation patterns.[1,2]

Techniques for calculating the transfer of electromagnetic radiation through clouds of particles have been summarized by Plass et al.[3] All of them require a knowledge of the scattering and absorption properties of the individual particles either for single scattering or, in the case of optically thick clouds, multiple scattering. Since each scattering event can affect the polarization by producing an electric field orthogonal to the incident field as well as parallel to it, an accurate treatment of the transfer problem must involve the complete scattering and absorption matrices for a single particle.

When the cloud particles are roughly spherical as they are for water droplets, it is not unreasonable to model them as spheres, and results obtained from the classical Mie theory[4] are then in good agreement with measured data. With ice crystals, however, a wide variety of shapes and sizes have been observed in clouds (see, for example, Aufm Kampe and Weickman[5]; Ono[6]). Plate crystals, i.e., cylinders of length much less than their diameter, and columnar (long thin) crystals, hollow as well as solid and of hexagonal cross-section, are quite commonly found, and for shapes as varied as these a sphere cannot provide an accurate simulation of the scattering. Nevertheless, for lack of any other applicable method, it has been customary to model these crystals using spheres of some equivalent radius, thereby introducing unknown

and possibly large errors in the values for the radiation transfer, which are the end products of extensive and expensive computations[7].

The importance of using the proper scattering matrix when the particles are irregular is clear from the data presented by Holland and Gagné[8]. They measured the matrix elements for clouds of irregularly shaped, randomly oriented silicon flakes, and found results quite different from those predicted by Mie theory, particularly for back and forward scatter.

The last few years have seen several attempts at calculating the scattering from more realistically-shaped crystals, and it is appropriate to mention here the work of Jacobowitz[9] and Liou[10-12] directed at the scattering properties of columnar ice crystals. Jacobowitz's data were obtained for infinitely long hexagonal crystals using ray tracing. Diffraction produced, for example, by the six longitudinal edges of the cylinder, was necessarily omitted, as well as the effect of polarization, and the calculations were limited to cylinders not less than 40 $\mu$m in diameter (at a wavelength of 0.55 $\mu$m) with the apparent objective of assuring the reasonable validity of geometrical optics. Finally, no account was taken of internal absorption by the ice in spite of the fact that the appreciable imaginary part of the refractive index at some infrared wavelengths suggests that absorption may not be negligible.

Liou's analyses are based on the assumption that the crystal can be modelled by an infinitely long homogeneous dielectric cylinder of circular cross section. Although this obviously suppresses those features of the scattering which are peculiar to the hexagonal cross section of an actual ice crystal, there is now a mathematically exact expression for the scattered field as a sum over orthogonal functions analogous to the Mie series for a sphere. It is therefore possible to compute the scattering precisely with all polarization information present and internal absorption taken into account.

The retention of the hexagonal geometry is a key feature of the present work, and in contrast to a circular cylinder, there is no exact expansion available for this shape. However, an integral equation approach has been developed with which to compute

the scattering from thin cylindrical dielectric shells of arbitrary cross section when irradiated by a plane wave of any polarization incident in a plane perpendicular to the generators. By applying the method to infinitely long hexagonal cylinders, scattering and absorption data have been generated applicable to hollow columnar (sheath) ice crystals in the infrared. To display the role played by the hexagonal geometry, these data have also been compared with the analogous results for hollow circular cylinders of equivalent dimensions.

## 2. Analysis

The method that we shall use originated from a study[13] of the scattering by dielectric and absorbing layers in which the layers were approximated by impedance sheets or membranes of infinitesimal thickness. According to this approximation, a layer of thickness $\tau$ composed of a material whose complex relative permittivity is $\epsilon_r$ and whose permeability is the same as that of the surrounding free space medium is represented as an infinitesimally thin membrane having complex impedance

$$\eta = \frac{iZ\lambda}{(\epsilon_r - 1)2\pi\tau} \tag{1}$$

ohms per square, where Z is the intrinsic impedance of free space and $\lambda$ is the free space wavelength. Mks units are employed and a time factor $e^{-i\omega t}$ suppressed. The resulting membrane is just an electric current sheet subject to the conditions

$$\left[\hat{n} \wedge \underline{E}\right]_-^+ = 0$$

$$\left[\hat{n} \wedge \underline{H}\right]_-^+ = \underline{J}$$

$$\hat{n} \wedge \left(\hat{n} \wedge \underline{E}\right) = -\eta \underline{J} \tag{2}$$

at its surface, where $\hat{n}$ is a unit vector (outward) normal to the side indicated by the plus sign and $\underline{J}$ is the total electric current supported.

This type of sheet has proved useful in a variety of problems, but it is only an approximation to a layer of non-zero thickness. It ignores[14] components of volume currents perpendicular to a layer as well as variations of the tangential components within the layer, but from analytical and numerical comparison of the results obtained with those for specific layers of non-zero thickness, it has been found accurate provided $\tau \lesssim 0.03\lambda$ and the sheet is located at the middle of the layer. Its great merit is that it allows us to simulate the scattering from a layer using a single surface current distribution, thereby making the problem of a sheath crystal relatively straightforward.

For generality, we consider a cylindrical membrane of infinite length with generators parallel to the z axis of a cylindrical polar coordinate system. The membrane has complex impedance $\eta$ ohms per square and is illuminated by a plane electromagnetic wave incident in a plane perpendicular to the z axis. Since there is no dependence on the z coordinate, the scattering problem is two dimensional and can be expressed as two scalar ones for the field components $E_z$ and $H_z$. It is therefore convenient to consider separately the cases of E and H polarizations in which the incident electric or magnetic field respectively is in the z direction.

Since the membrane supports no magnetic current, the scattered electric field can be represented in terms of the electric Hertz vector

$$\underline{\Pi}(\underline{\rho}) = -\frac{Z}{4k}\int_C \underline{J}(s')H_o^{(1)}(kR)ds' \tag{3}$$

as

$$\underline{E}^s(\underline{\rho}) = \nabla_\wedge\nabla_\wedge\underline{\Pi}(\rho), \tag{4}$$

where ds' is an element of arclength on the closed contour C constituting the perimeter of the cylinder in the plane $z = 0$. R is the distance between the field point and the point of integration, $k = 2\pi/\lambda$ and $H_o^{(1)}(kR)$ is the zero order Hankel function of the first kind.

For E polarization $\underline{E} = \hat{z}E_z$ implying $\underline{J} = \hat{z}J_z$, and when the vector differentiations are performed, it is found that

$$E_z^s(\underline{\rho}) = -\frac{kZ}{4}\int_C J_z(s')H_o^{(1)}(kR)ds'. \tag{5}$$

The total field is then $E_z^i + E_z^s$ and on allowing $\underline{\rho}$ to lie on C and applying the boundary condition (2), we have

$$E_z^i(s) = \eta J_z(s) + \frac{kZ}{4}\int_C J_z(s')H_o^{(1)}(kR)ds'. \tag{6}$$

This is a singular integral equation from which $J_z(s)$ can be obtained numerically by the moment method[15]. As always the contribution from the self cell containing the field point must be determined analytically, so that in effect (6) is replaced by

$$E_z^i(s) = \left[\eta + \frac{kZ\Delta}{4}\left\{1 + \frac{2i}{\pi}\left(\ell n\frac{\Delta}{\lambda} + 0.028798\ldots\right)\right\}\right]J_z(s) + \frac{kZ}{4}\int_{C-\Delta} J_z(s')H_o^{(1)}(kR)ds' \tag{7}$$

where $\Delta$ is the self cell of size $\Delta$. Having found $J_z(s)$, (5) can be used to compute the scattered field at any point in the plane $z = 0$.

The case of H polarization ($\underline{H} = \hat{z}H_z$) is more complicated because the current is now circumferential ($\underline{J} = \hat{s}J_s$), but by a process similar to the above we find

$$E_s^s(\underline{\rho}) = -\frac{kZ}{4}\int_C \left\{J_s(s')(\hat{s}\cdot\hat{s}') - \frac{1}{k^2}\frac{\partial}{\partial s'}J_s(s')\frac{\partial}{\partial s'}\right\}H_o^{(1)}(kR)ds'. \tag{8}$$

The total circumferential electric field is then $E_s^i + E_s^s$ and in the limit when the field point lies on the surface application of the boundary condition gives

$$E_s^i(s) = \eta J_s(s) + \frac{kZ}{4}\int_C \left\{J_s(s')(\hat{s}\cdot\hat{s}')H_o^{(1)}(kR) - \frac{1}{k}\frac{\partial}{\partial s'}J_s(s')(\hat{s}\cdot\hat{R})H_1^{(1)}(kR)\right\}ds' \tag{9}$$

where $\hat{R}$ is a unit vector directed from the point of integration to the field point. This is a valid integral equation for the circumferential current $J_s(s)$ but is complicated by

the presence of the surface derivative of the current. On the other hand, by a process equivalent to an integration by parts, (8) can be written as

$$E_s^s(\rho) = -\frac{kZ}{4}\int_C J_s(s')\left\{(\hat{s}\cdot\hat{s}') + \frac{1}{k^2}\frac{\partial^2}{\partial s'^2}\right\}H_o^{(1)}(kR)ds' \qquad (10)$$

leading to the integral equation

$$E_s^i(s) = \eta J_s(s) + \frac{kZ}{4}\int_C J_s(s')(\hat{s}\cdot\hat{s}')H_o^{(1)}(kR)ds'$$

$$+\frac{Z}{4}\lim_{\rho\to C}\int_C J_s(s')\frac{\partial}{\partial s'}\left\{(\hat{s}\cdot\hat{R})H_1^{(1)}(kR)\right\}ds' \qquad (11)$$

in which only the unknown current $J_s(s)$ appears.

This simplification has its price. Because of the high order singularity of the second integrand in (11), it is no longer possible to reverse the order of the limit and integral operations unless we segment the range of integration prior to taking the limit and then maintain the segment or cell size $\Delta \neq 0$. This is, of course, no restriction as regards a numerical solution. If $\Delta$ is the self cell, an analytical evaluation then shows

$$\lim_{\rho\to C}\int_\Delta \ldots\ ds' = \left[\frac{8i}{\pi k\Delta} - \frac{k\Delta}{2}\left\{1 + \frac{2i}{\pi}\left(\ln\frac{\Delta}{\lambda} + 0.528798 + \ldots\right)\right\}\right]J_s(s).$$

and

$$\lim_{\rho\to C}\int_{C-\Delta} \ldots .ds' = \sum_{\substack{j=1\\ j\neq i}}^{N} J_s(s_j)\left[(\hat{s}\cdot\hat{R})H_1^{(1)}(kR)\right]_{s' = s_j - \Delta/2}^{s' = s_j + \Delta/2}$$

where we have assumed the current constant over each of the N cells into which the profile C has been divided. By also evaluating the self cell contribution of the first integral in (11) in the same manner as we did for (6), our integral equation becomes

$$E_s^i(s) = \left[\eta + \frac{2iZ}{\pi k\Delta} + \frac{kZ\Delta}{8}\left\{1 + \frac{2i}{\pi}\left(\ln\frac{\Delta}{\lambda} - 0.471202\ldots\right)\right\}\right] J_s(s)$$

$$+ \frac{kZ}{4}\int_{C-\Delta} J_s(s')(\hat{s}\cdot\hat{s}')H_o^{(1)}(kR)\,ds'$$

$$+ \frac{Z}{4}\sum_{\substack{j=1\\ j\neq i}}^{N} J_s(s_j)\left[(\hat{s}'\cdot\hat{R})H_1^{(1)}(kR)\right]_{s' = s_j - \Delta/2}^{s' = s_j + \Delta/2} \qquad (12)$$

Although the coefficient of $J_s(s)$ in the first term on the right hand side becomes infinite as $\Delta \to 0$, the equation is quite amenable to numerical solution, and the results obtained are (perhaps surprisingly) insensitive to $\Delta$ for a wide range of cell sizes. We have, in fact, used this equation in a number of applications, and it will also be used here.

For an E-polarized incident plane wave,

$$E_z^i = \exp\left\{-ik(x\cos\phi_o + y\sin\phi_o)\right\} \qquad (13)$$

where $\pi + \phi_o$ is the angle which the direction of propagation makes with respect to the x axis. Once $J_z(s)$ has been found from (7), the scattered electric field in the far zone of the cylinder is

$$E_z^s = \sqrt{\frac{2}{\pi k\rho}}\, e^{i(k\rho - \pi/4)} A_e(\phi, \phi_o)$$

where the complex scattering amplitude $A_e$ is given by

$$A_e(\phi, \phi_o) = -\frac{kZ}{4}\int_C J_z(s')e^{-ik\hat{\rho}\cdot\underline{\rho}'}\,ds', \qquad (14)$$

and

$$\hat{\rho} = \hat{x}\cos\phi + \hat{y}\sin\phi$$

is a unit vector in the direction of observation. The backscattering direction is therefore $\phi = \phi_o$. In terms of $A_e$, the two dimensional bistatic scattering cross section or phase function is

$$\sigma(\phi, \phi_o) = \frac{4}{k} |A_e(\phi, \phi_o)|^2 . \tag{15}$$

If the incident plane wave is H-polarized, $H_z^i$ now has the form shown in (13), and having obtained $J_s(s)$ from (12), the scattered magnetic field in the far zone is given by

$$H_z^s = \sqrt{\frac{2}{\pi k\rho}}\, e^{i(k\rho - \pi/4)}\, A_h(\phi, \phi_o)$$

where

$$A_h(\phi, \phi_o) = -\frac{k}{4}\int_C (\hat{\rho}\cdot\hat{n}')J_s(s')e^{-ik\hat{\rho}\cdot\rho'}\, ds' . \tag{16}$$

The H-polarized cross section can be found using (15) with $A_h$ replacing $A_e$.

Two quantities of particular interest are the total (integrated) scattering cross section $\sigma_T$ and the absorption cross section $\sigma_A$. The former is given by

$$\sigma_T(\phi_o) = \frac{1}{2\pi}\int_0^{2\pi} \sigma(\phi, \phi_o)d\phi \tag{17}$$

and if this integral is confined to the ranges $0 - \pi$ or $\pi - 2\pi$ we have the forward or backward power fluxes. From the foward scattering theorem, the absorption cross section is

$$\sigma_A(\phi_o) = -\sigma_T(\phi_o) - \frac{4}{k}\,\mathrm{Re.}\, A(\pi + \phi_o, \phi_o) . \tag{18}$$

The extinction cross section is then the sum

$$\sigma_E(\phi_o) = \sigma_T(\phi_o) + \sigma_A(\phi_o) \tag{19}$$

We remark that for a cylinder of finite length $\ell \gtrsim \lambda$, each three-dimensional cross section $\sigma^{(3)}$ for incidence in a plane perpendicular to the length, computed on the

assumption that the surface field is the same as for the infinite cylinder, is related to the corresponding two-dimensional cross section $\sigma$ by

$$\sigma^{(3)} = \frac{2\ell^2}{\lambda}\sigma . \tag{20}$$

## 3. Computed Data

Computer programs have been written to solve the integral equations (7) and (12) respectively and, hence, determine the various cross sections for any cylindrical membrane whose profile is made up of straight line and circular arc segments. Data have been generated for circular and hexagonal cylindrical shells having a variety of dimensions (including thickness) and for the refractive index of ice over a wide range of frequencies in the infrared. In the case of the hexagon, two directions of plane wave incidence were considered: edge-on and face-on, i.e., along a bisector of the angle at an edge and normal to a face respectively. The majority of the data were for a hexagon $3\mu$m on a face with a wall thickness $0.1\mu$m and we present only these data here. The number N of sampling points used in the computer program ranged from 96 at the shorter wavelengths to 30 at the longer. The program is described in Weil and Senior[16] where additional data can be found.

We have also used the program to generate results for hollow circular cylinders of the same thickness $\tau = 0.1\mu$m and with radii equal to (i) $3\mu$m, the length of a face of the hexagon, and (ii) $9/\pi\ \mu$m, so that the hexagonal and circular cylinders have the same circumference. At the wavelengths $\lambda = 3.1$ and $12.5\mu$m the data for the circular cylinder have been compared with those for a cylindrical shell of outer and inner radii $9/\pi \pm 0.05\mu$m computed using the orthogonal function (or Mie series) expansion of the scattered field. For the refractive indices used, the bistatic scattering cross sections agreed to within 0.2 dB for E-polarization, but showed somewhat larger ($\sim$1.0 dB) discrepancies for H-polarization.

The refractive indices were taken from Irvine and Pollack[17] (IP) and Schaaf and Williams[18] (SW), and are plotted in Figure 1. There are noticable differences at certain wavelengths and to see the effect that they produce, computations at $\lambda = 2.25$ and $3.0\mu$m were carried out for the refractive indices from both references.

Angular cross section data for $\lambda$ = 3.1 and 12.5$\mu$m are presented in Figure 2. As expected, the number of maxima and minima in $0 \leq \phi \leq \pi$ increases with decreasing $\lambda$, and at wavelengths which are much longer than the face length of the hexagon, e.g., $\lambda \gtrsim 8\mu$m, the cross section has almost no angular structure. Changing the incidence from edge-on to face-on has most effect in directions close to backscattering, and we note the substantial differences between the results for E and H polarizations. The results for corresponding circular cylinders have been included in the figures to demonstrate the importance of using the exact cross sectional shape. The locations and magnitudes of the extrema differ for the two types of body, and though the curves are similar in certain angular ranges, they are far apart in others.

The values of $\sigma_T$, $\sigma_A$ and $\sigma_E$ for the cases shown in Figure 2 are listed in Table 1. For a fixed wavelength, it would appear that the absorption is primarily volume rather than shape dependent.

Spectral data for the cross sections $\sigma(0)$, $\sigma(\pi)$, $\sigma_T$ and $\sigma_A$ of the hexagonal cylinder are given in Figures 3 and 4. Each figure has two parts covering the ranges 1.6 to 3.5$\mu$m and 8 to 12.5$\mu$m. Separate curves are shown wherever the results for edge-on and face-on are clearly distinguishable. For the most part this is only true of the backscattering cross section $\sigma(0)$, and in the other figures the differences are confined to the immediate vicinity of local maxima and minima.

In the longer wavelength range the SW values for the refractive index were employed, but most of the data at the shorter wavelengths were computed using the IP values. The latter range spans the main absorption band centered on $\lambda$ = 3$\mu$m and the secondary one at $\lambda$ = 2$\mu$m. These wavelengths show the main discrepancies between the IP and SW values and here we ran the data for both sets of refractive index. As Figures 3 and 4 show, the discrepancies do produce substantial differences in the cross sections.

The geometrical effects are particularly pronounced for $\lambda \lesssim 3.5\mu$m. This is not surprising since the dimensions of the cylinder are now comparable to a wavelength, or a low multiple thereof, and this is the region where resonance effects and other

interactions between the various contributors to the scattering are most important. As an example, while $\sigma_A$ has a strong local maximum near the maximum in $n_i$ at $\lambda = 3.075\,\mu m$, the shape and overall width of the maximum in $\sigma_A$ are apparently affected by the fact that the side length of the hexagon is now almost a wavelength. $\sigma(0)$ and $\sigma(\pi)$ both show a corresponding drop in this absorption region. The behavior is quite different near the secondary maximum in $n_i$ at $\lambda = 2\,\mu m$. For H-polarization but not for E, $\sigma_A$ is large as expected, while $\sigma(0)$ and $\sigma(\pi)$ have local maxima for $\lambda$ just above $2\,\mu m$ with both polarizations.

Further evidence for the way in which a geometrical effect can dominate a material absorption effect can be found by comparing the absorption cross sections at $2.25\,\mu m$ computed from the IP and SW data. At this wavelength the SW value for $n_i$ is roughly five times the IP value, with $n_r$ almost equal in both sets of data, but the SW value produces an absorption cross section which is an order of magnitude less than that given by the IP value. It is therefore obvious that predictions of absorption and scattering based only on the properties of the material of which the scatterer is composed may be considerably in error.

Acknowledgements

This work was supported by NASA Grant 5044 and in part by AFOSR Grant 72-2262.

| Cylinder Type and Irradiation | | wavelength ($\mu$m) | $\sigma_T/\lambda$ | $\sigma_A/\lambda$ | $\sigma_E/\lambda$ |
|---|---|---|---|---|---|
| hex, 3$\mu$m side, edge-on, | E polarization | 3.1 | -7.74 | -1.29 | -0.40 |
| | H polarization | 3.1 | -12.16 | -4.10 | -3.47 |
| | E polarization | 12.5 | -23.76 | -10.97 | -10.75 |
| | H polarization | 12.5 | -29.09 | -13.45 | -13.82 |
| hex, 3$\mu$m side, face-on, | E polarization | 3.1 | -7.97 | -1.22 | -0.37 |
| | H polarization | 3.1 | -12.88 | -4.06 | -3.52 |
| | E polarization | 12.5 | -23.77 | -10.97 | -10.75 |
| | H polarization | 12.5 | -29.12 | -13.95 | -13.82 |
| circular, rad = hex side, | E polarization | 3.1 | 0.00 | 2.27 | 4.30 |
| | H polarization | 3.1 | -3.75 | 0.65 | 1.99 |
| | E polarization | 12.5 | -23.59 | -10.76 | -10.55 |
| | H polarization | 12.5 | -27.55 | -13.74 | -13.57 |
| circular, | E polarization | 3.1 | -8.11 | -1.16 | -0.36 |
| perim = hex perim, | H polarization | 3.1 | -12.77 | -3.95 | -3.42 |
| | E polarization | 12.5 | -23.89 | -10.96 | -10.74 |
| | H polarization | 12.5 | -28.19 | -13.72 | -13.76 |

Table 1. Total, absorption and extinction cross sections of cylindrical shell ice cylinders 0.1$\mu$m thick for two infrared wavelengths: $\lambda = 3.1\mu$m with [17] $n = 1.280 + i\,0.3252$ and $\lambda = 12.5\mu$m with [18] $n = 1.387 + i\,0422$.

## References


1. S. K. Cox, J. Atmos. Sci., 28, 1513 (1971).
2. ARWG, Bull. Amer. Meteo. Soc., 53, 950 (1972).
3. G. N. Plass, G.W. Kattawar and F.E. Catchings, Appl. Opt., 12, 314 (1973).
4. J. A. Stratton, Electromagnetic Theory (McGraw-Hill, New York, 1941).
5. H. J. AumfKampe and H.K. Weickman, Meteo. Res. Revs., Summaries of Progress from 1951 - 1955, 3 (1955).
6. A. Ono, J. Atmos. Sci., 26, 138 (1969).
7. G. W. Kattawar and G.N. Plass, Appl. Opt., 11, 2851 (1972).
8. A. C. Holland and G. Gagné, Appl. Opt., 9, 1113 (1970).
9. H. Jacobowitz, J. Quant. Spectrosc. Radiat. Transfer, 11, 691 (1971).
10. K.-N. Liou, Appl. Opt., 11, 667 (1972).
11. K.-N. Liou, J. Atmos. Sci., 29, 524 (1972).
12. K.-N. Liou, J. Geophys. Res., 78, 1409 (1973).
13. E. F. Knott, and T.B.A. Senior, University of Michigan Radiation Laboratory Report No. 0110764-1-T, Ann Arbor, MI. (1974).
14. R. F. Harrington and J.R. Mautz, IEEE Trans. AP-23, 531 (1975).
15. R. F. Harrington, Field Computations by Moment Methods (Macmillan, New York, 1968).
16. H. Weil and T.B.A. Senior, University of Michigan Radiation Laboratory Report No. 013381-1-F, Ann Arbor, MI. (1976).
17. W. M. Irvine, and J.B. Pollack, Icarus, 8, 324 (1968).
18. J. W. Schaff and D. Williams, J. Opt. Soc. Amer., 63, 726 (1973).

## Figure Captions

Figure 1. Refractive index of ice in the infrared. The solid line represents data from Irvine and Pollack[17], the ⊖ points represent data from Schaff and Williams[18]: (a) real part of refractive index minus one vs. wavelength; (b) imaginary part of refractive index vs. wavelength.

Figure 2. Angular distribution of the normalized scattering cross section $\sigma(\phi, \phi_o)/\lambda$ vs. $\phi$ for fixed incidence angle $\phi_o$: ——— hexagonal shell cylinder 3$\mu$m on a side irradiated edge-on; — - - - — same cylinder irradiated edge-on; - - - - circular shell cylinder of radius equal to the side length of the hexagon; — — — circular shell cylinder of same perimeter length as the hexagon. Each cylinder has a simulated 0.1 $\mu$m wall thickness. (a) wavelength $\lambda$ = 3.1 $\mu$m, E-polarization; (b) $\lambda$ = 3.1 $\mu$m, H-polarization; (c) $\lambda$ = 12.5 $\mu$m, E-polarization; (d) $\lambda$ = 12.5 $\mu$m, H-polarization. The refractive index values used are n = 1.280 + i0.3252 for[17] $\lambda$ = 3.1, and n = 1.387 + i0.422 for[18] $\lambda$ = 12.5.

Figure 3. Scattering cross sections of hexagonal shell cylinders vs. wavelength, wall thickness 0.1 $\mu$m; · edge-on, ⊖ face-on irradiation for Irvine and Pollack[17] refractive index data; x edge-on, ⊗ face-on irradiation for Schaaf and Williams[18] refractive index data: (a) backscatter, E-polarization; (b) backscatter, H-polarization; (c) forward scatter, E-polarization; (d) forward scatter, H-polarization.

Figure Captions (Continued)

Figure 4. Total absorption cross sections of hexagonal shell cylinders for data of Figure 3. (a) total scattering, E-polarization; (b) total scattering, H-polarization; (c) absorption, E-polarization, (d) absorption, H-polarization.

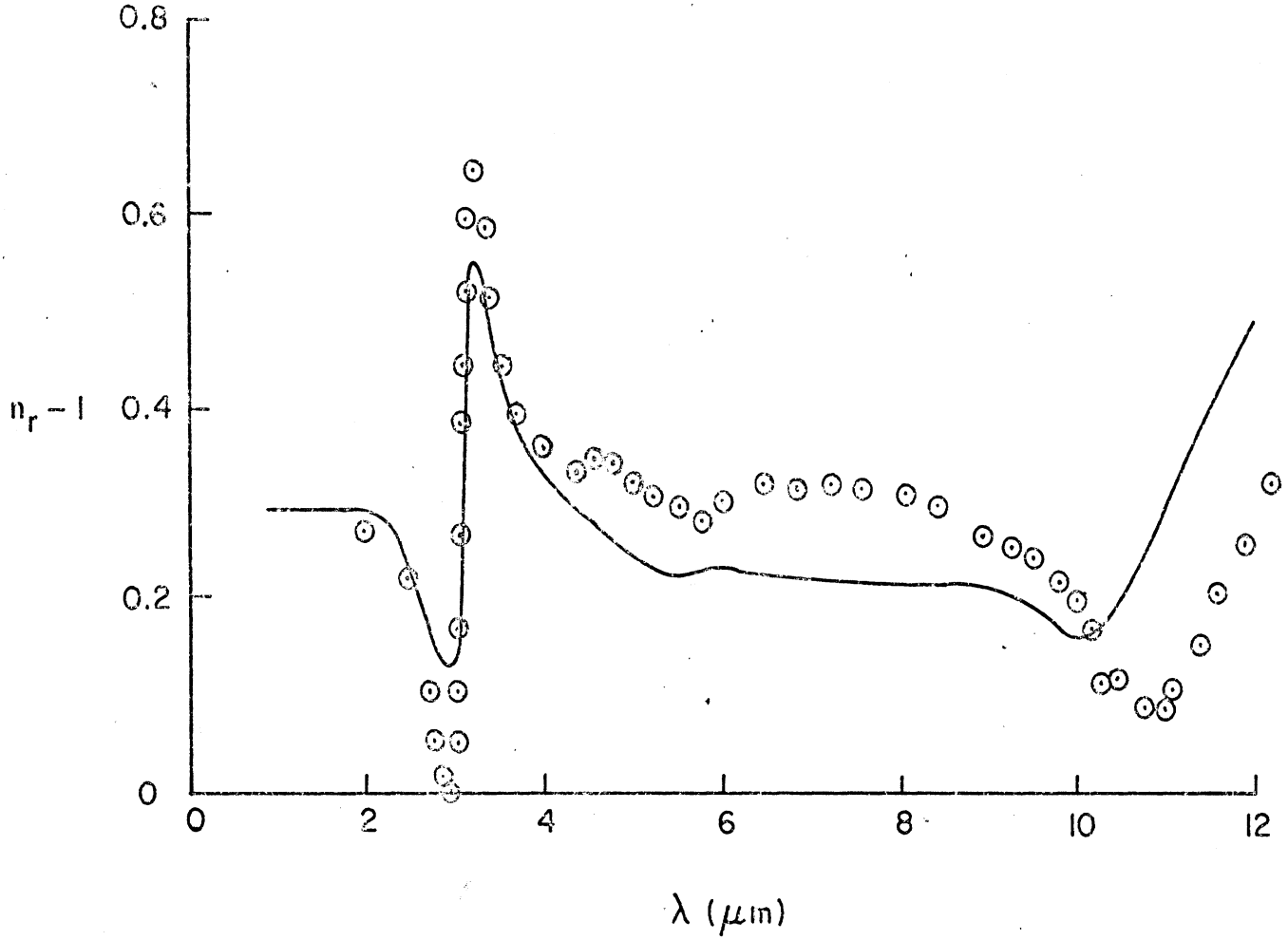
0.8
0.6
0.4
0.2
0
$n_r - 1$
0
2
4
6
8
10
12
λ (μm)

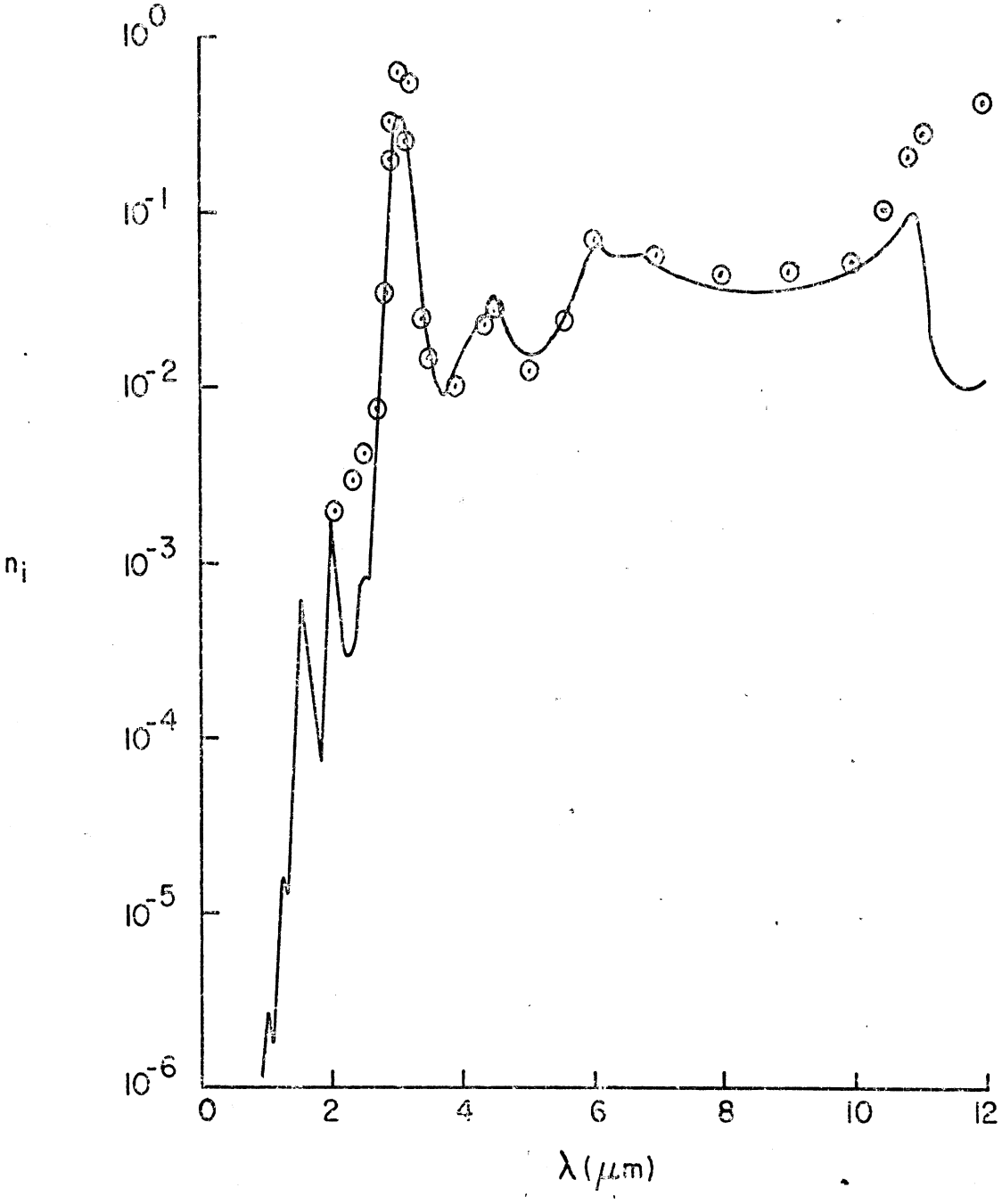
$10^{0}$
$10^{-1}$
$10^{-2}$
$10^{-3}$
$10^{-4}$
$10^{-5}$
$10^{-6}$
$n_i$
0
2
4
6
8
10
12
λ (μm)

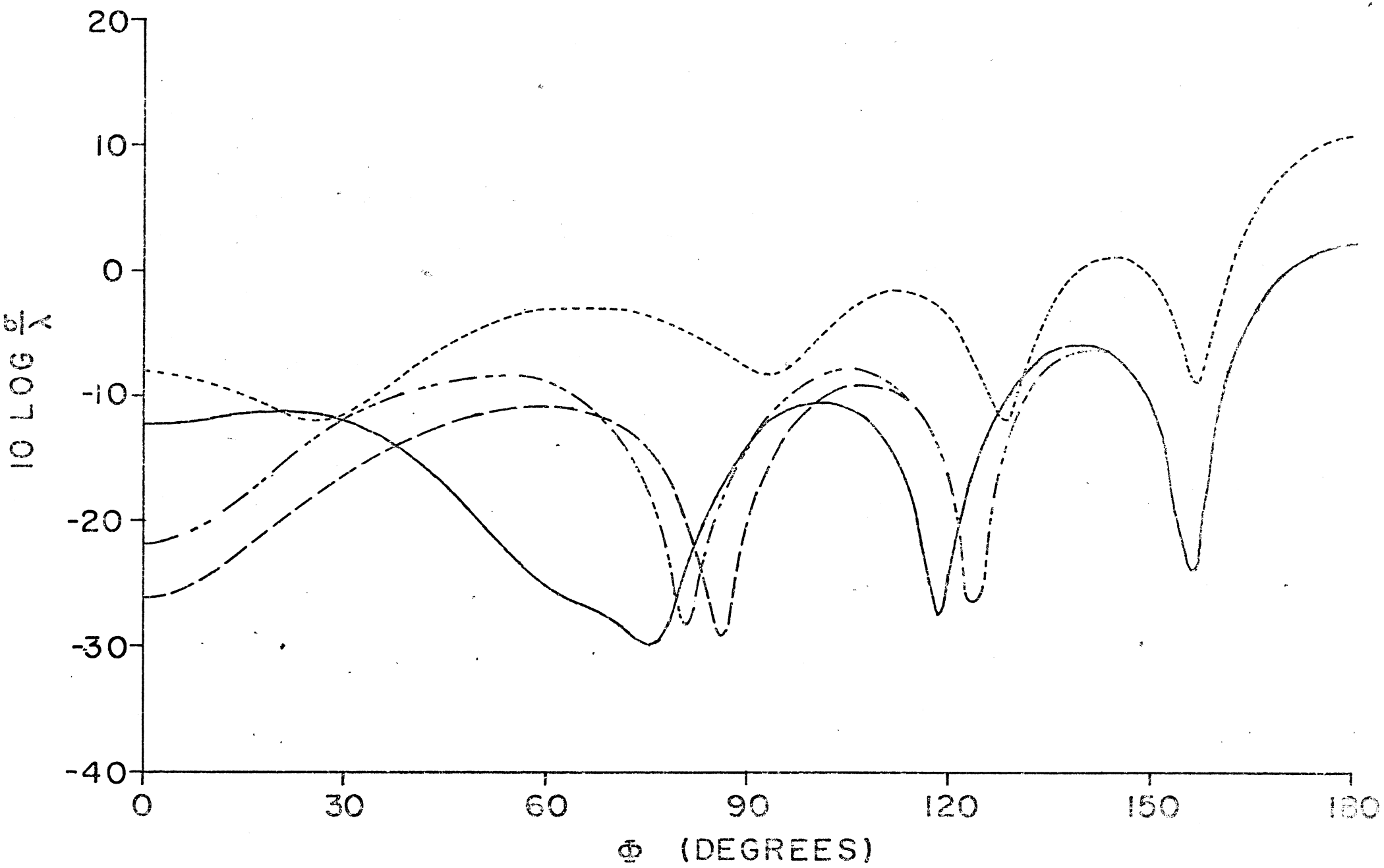
20
10
0
-10
-20
-30
-40
10 LOG σ/λ
0
30
60
90
120
150
180
Φ (DEGREES)

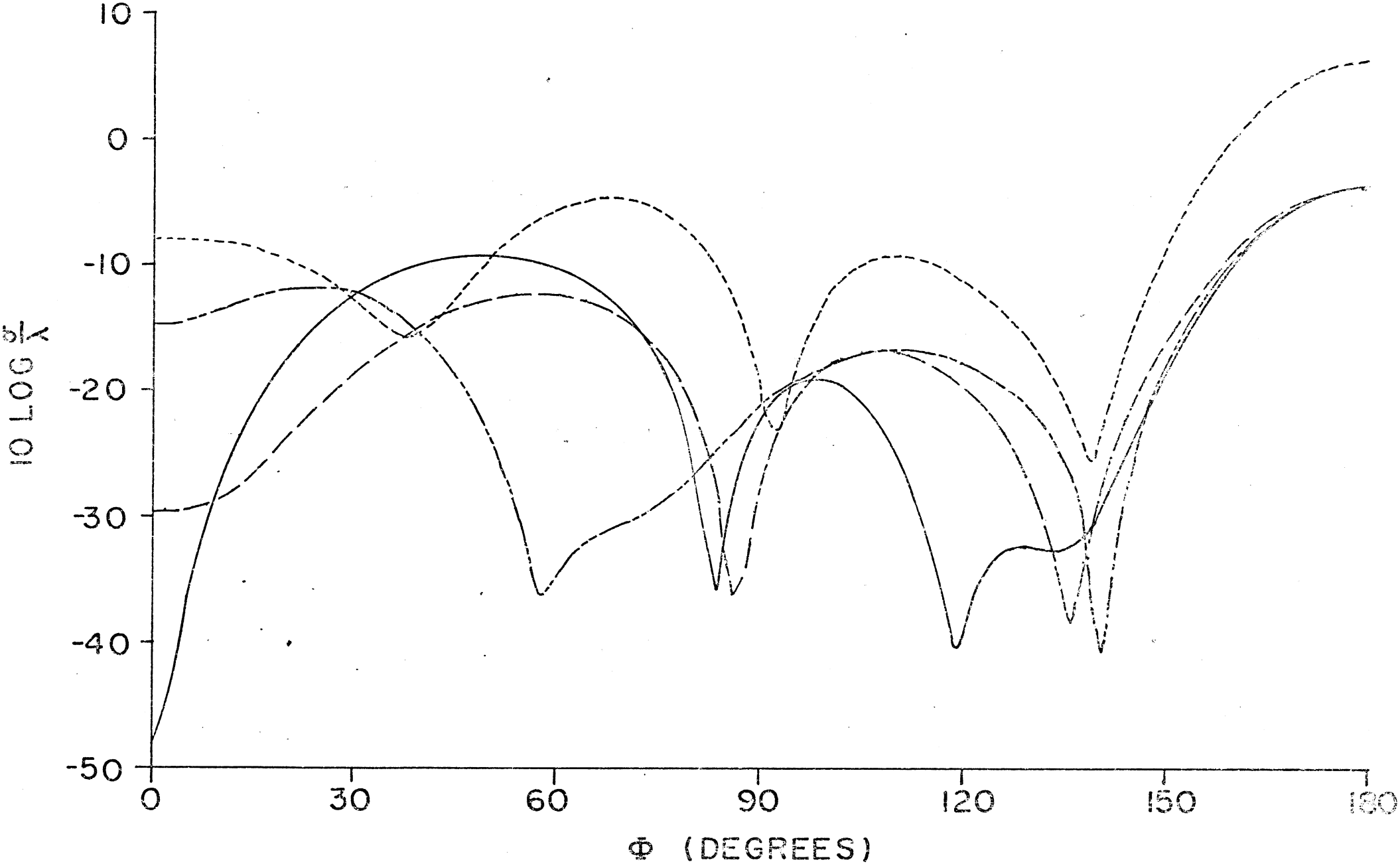
10
0
-10
-20
-30
-40
-50
10 LOG σ/λ
0
30
60
90
120
150
180
Φ (DEGREES)

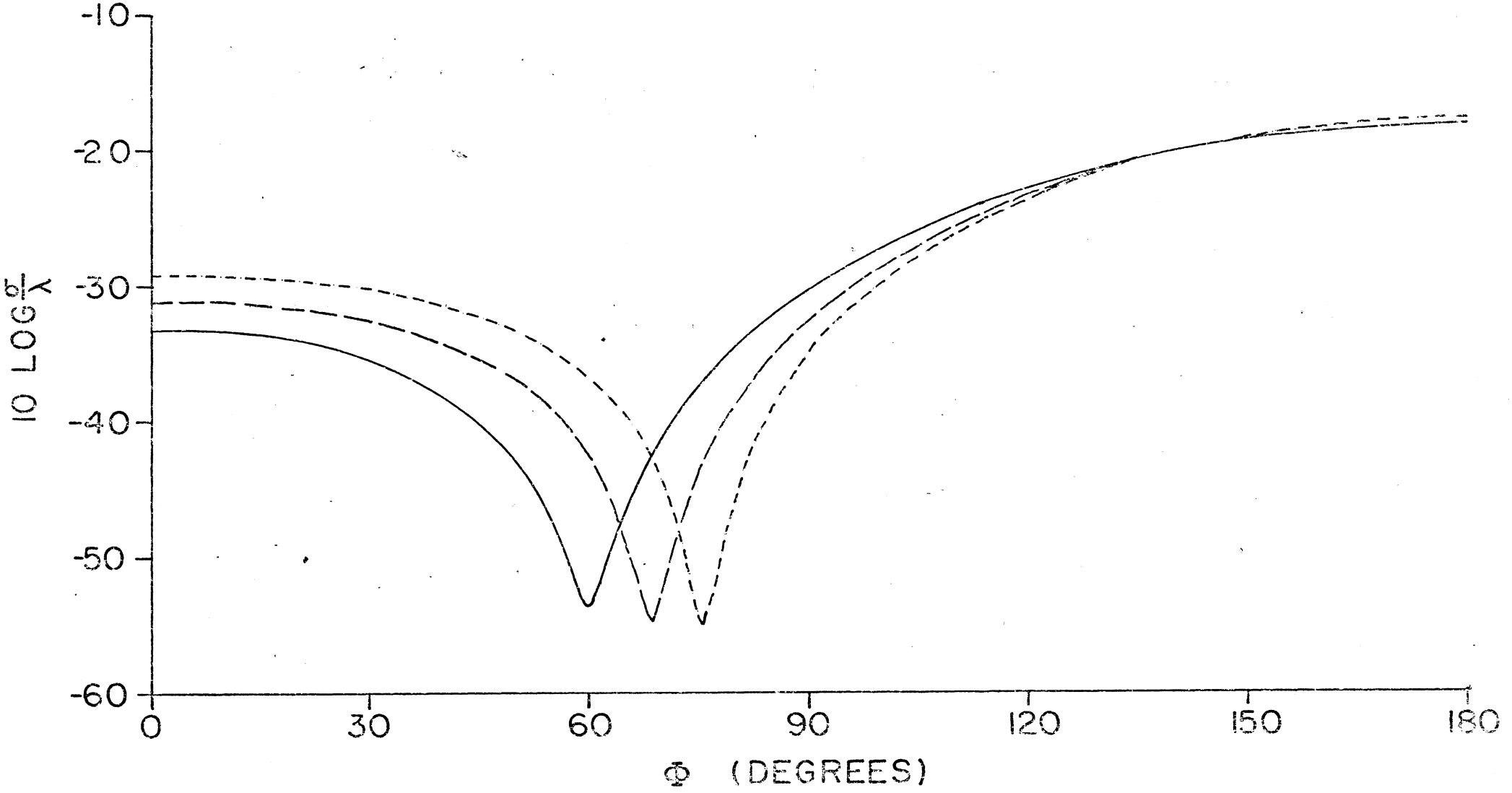
-10
-20
-30
-40
-50
-60
10 LOG σ/λ
0
30
60
90
120
150
180
Φ (DEGREES)

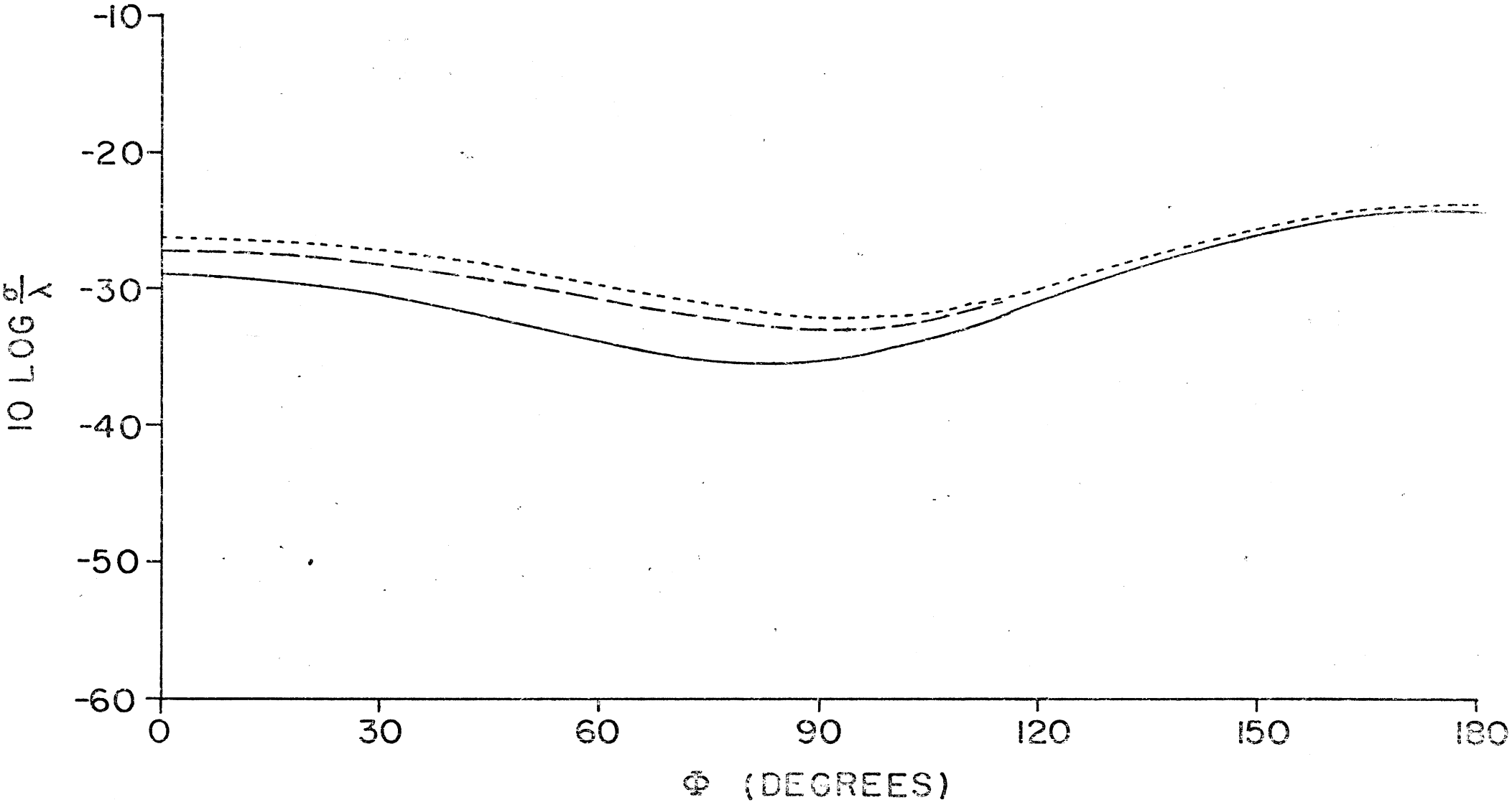
-10
-20
-30
-40
-50
-60
10 LOG σ/λ
0
30
60
90
120
150
180
Φ (DEGREES)

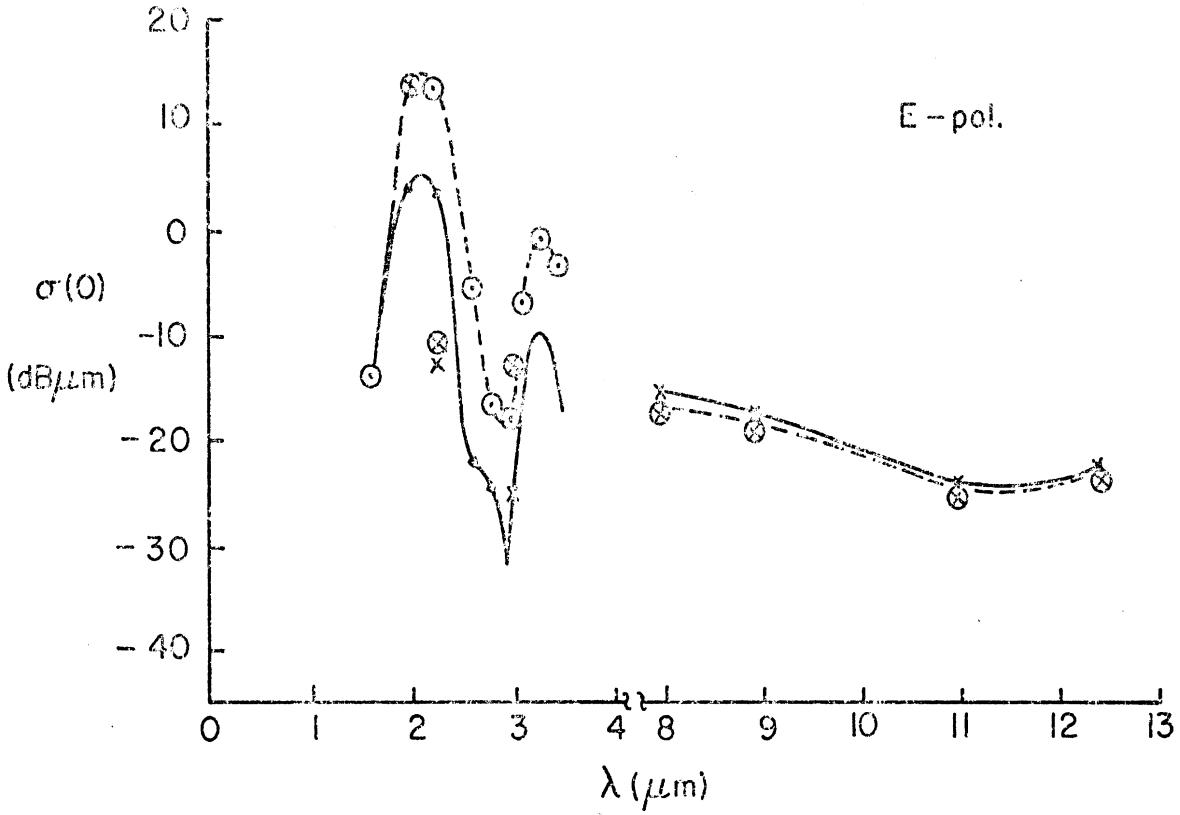
E – pol.
σ(0)
(dBμm)
20
10
0
-10
-20
-30
-40
0
1
2
3
4
8
9
10
11
12
13
λ (μm)

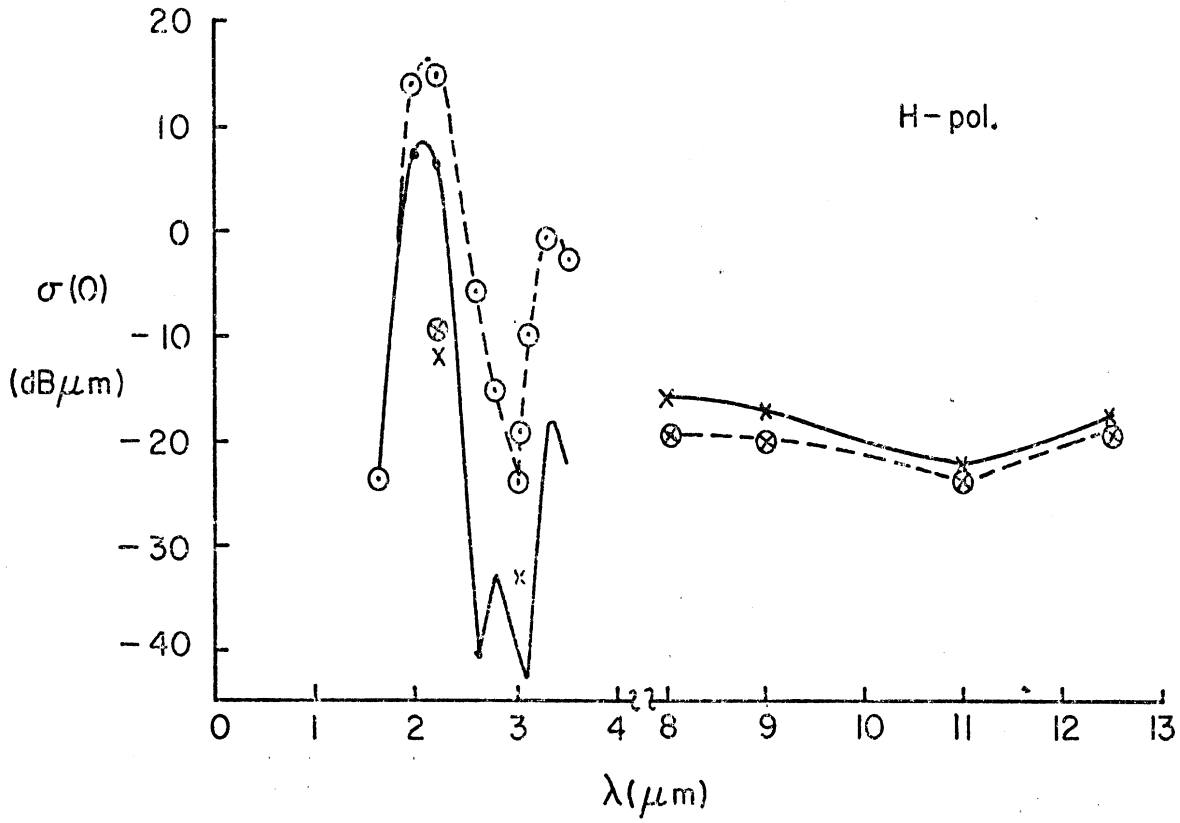
H – pol.
σ(0)
(dBμm)
20
10
0
-10
-20
-30
-40
0
1
2
3
4
8
9
10
11
12
13
λ(μm)

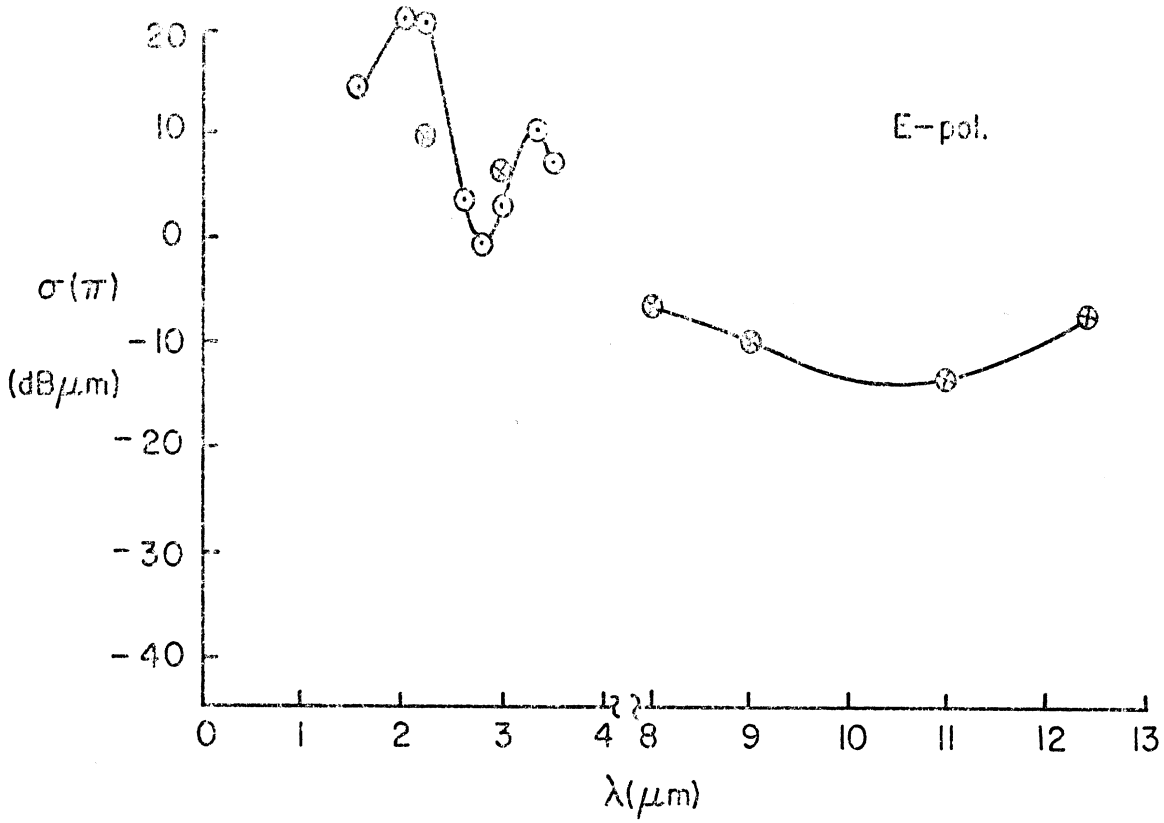
E-pol.
σ(π)
(dBμm)
20
10
0
-10
-20
-30
-40
0
1
2
3
4
8
9
10
11
12
13
λ(μm)

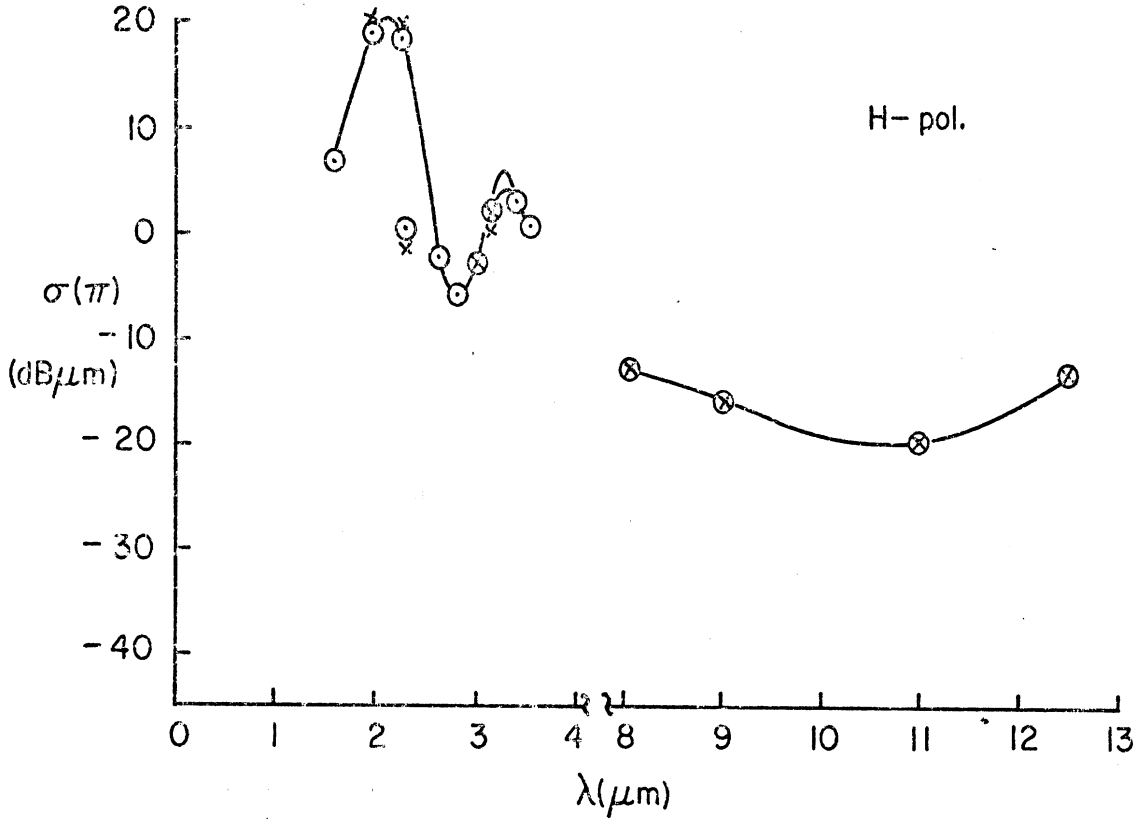
H-pol.
σ(π)
(dBμm)
20
10
0
-10
-20
-30
-40
0
1
2
3
4
8
9
10
11
12
13
λ(μm)

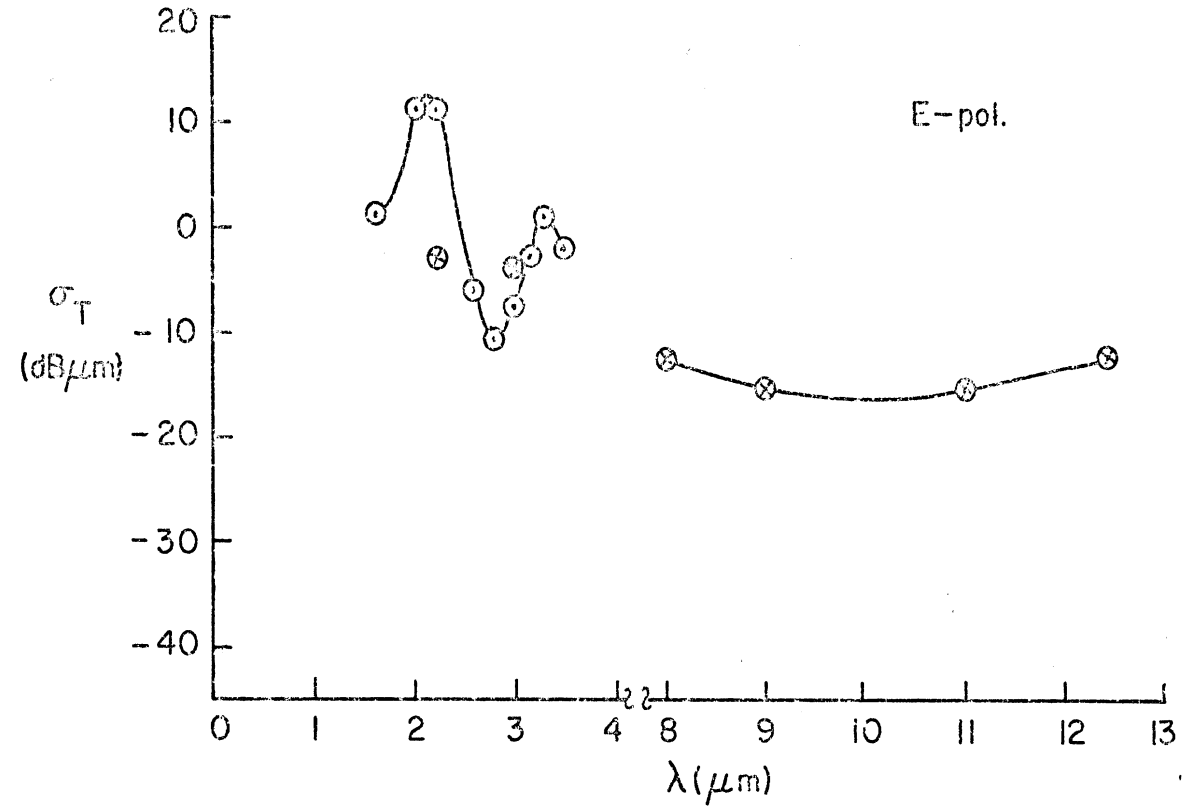
E-pol.
$\sigma_T$ (dBμm)
20
10
0
-10
-20
-30
-40
0
1
2
3
4
8
9
10
11
12
13
λ(μm)

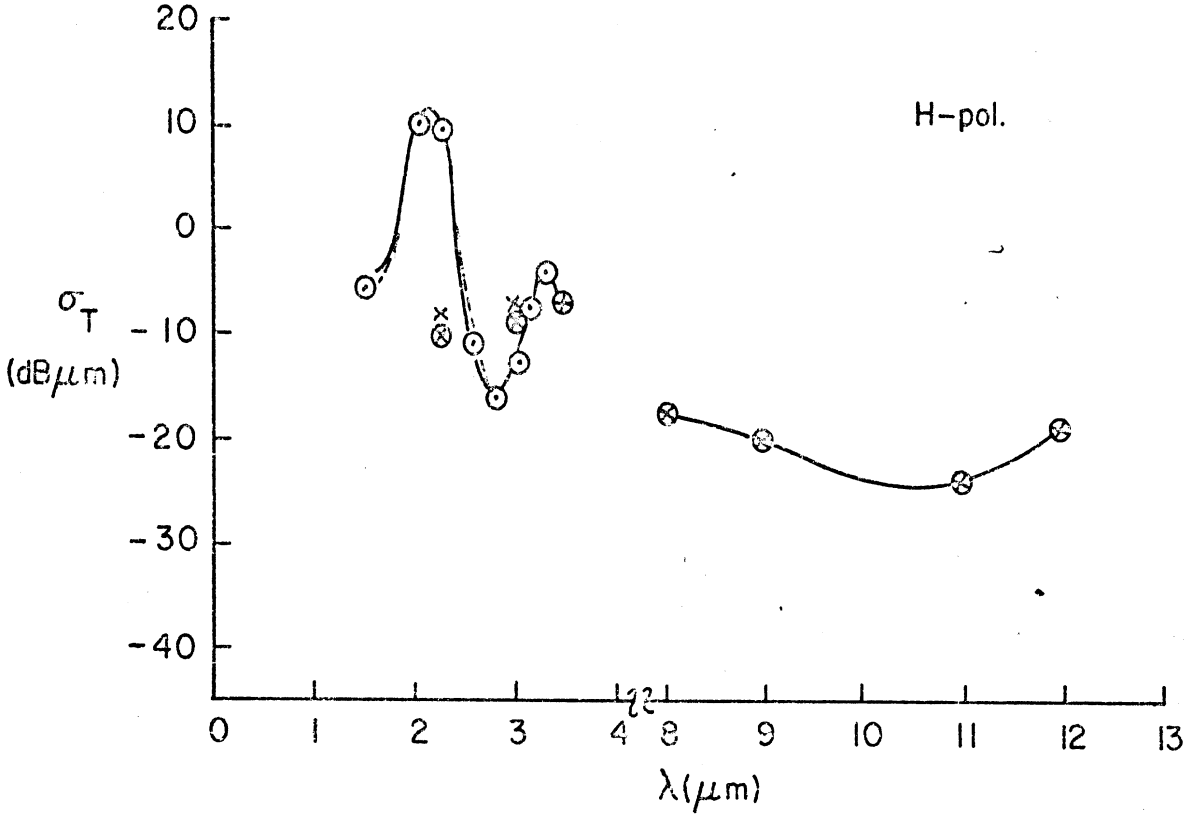
H-pol.
$\sigma_T$ (dBμm)
20
10
0
-10
-20
-30
-40
0
1
2
3
4
8
9
10
11
12
13
λ(μm)

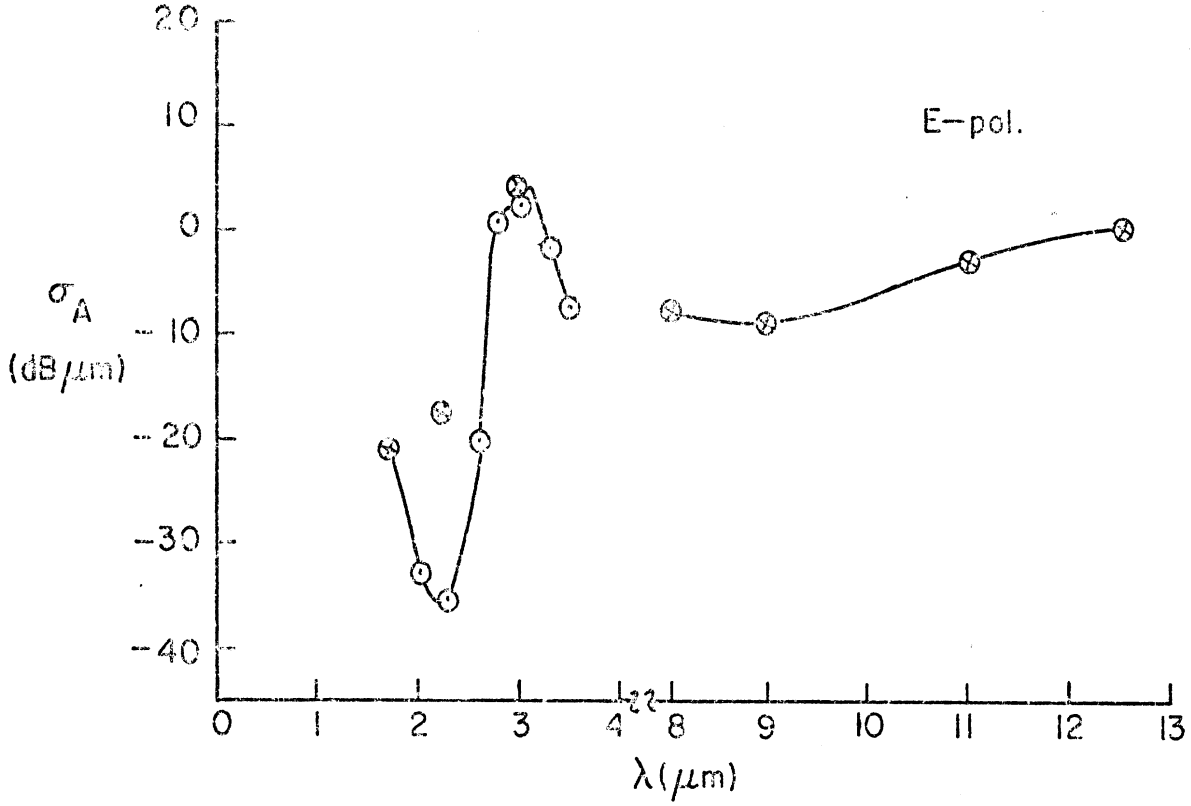
E–pol.
$\sigma_A$ (dB/μm)
20
10
0
-10
-20
-30
-40
0
1
2
3
4
8
9
10
11
12
13
λ(μm)

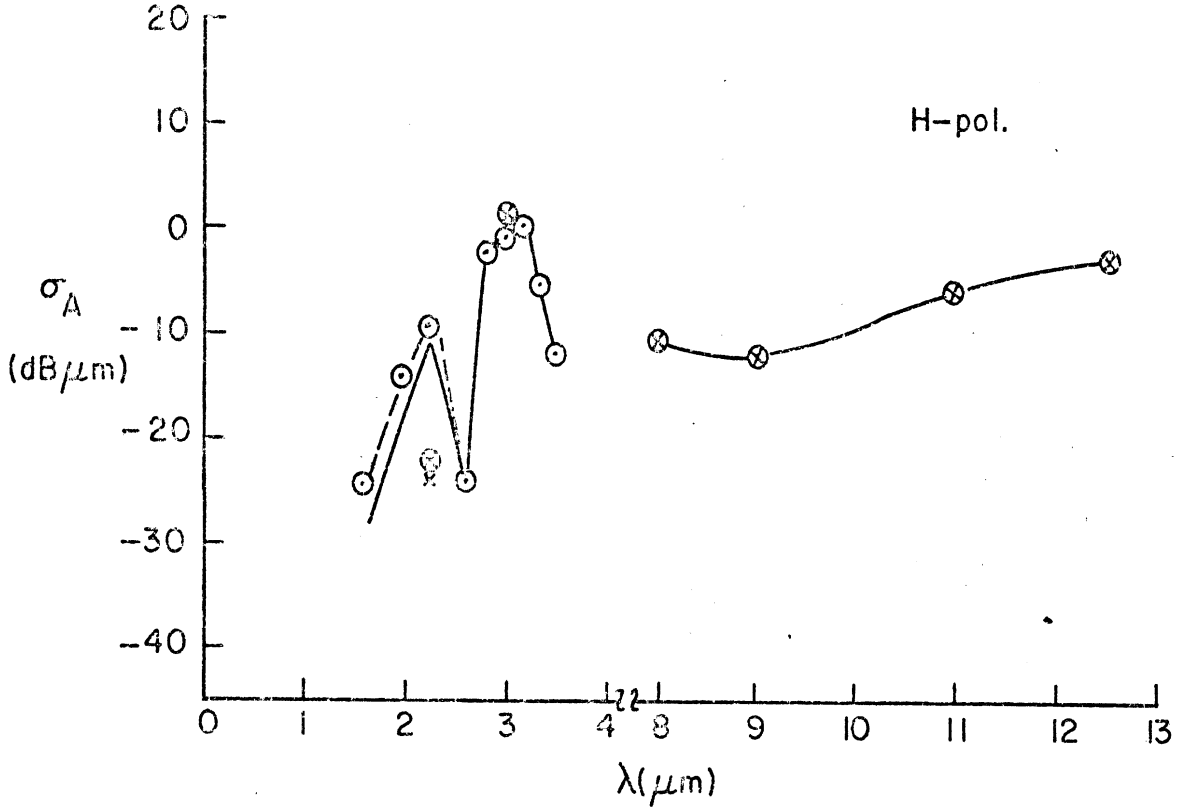
H–pol.
$\sigma_A$ (dB/μm)
20
10
0
-10
-20
-30
-40
0
1
2
3
4
8
9
10
11
12
13
λ(μm)

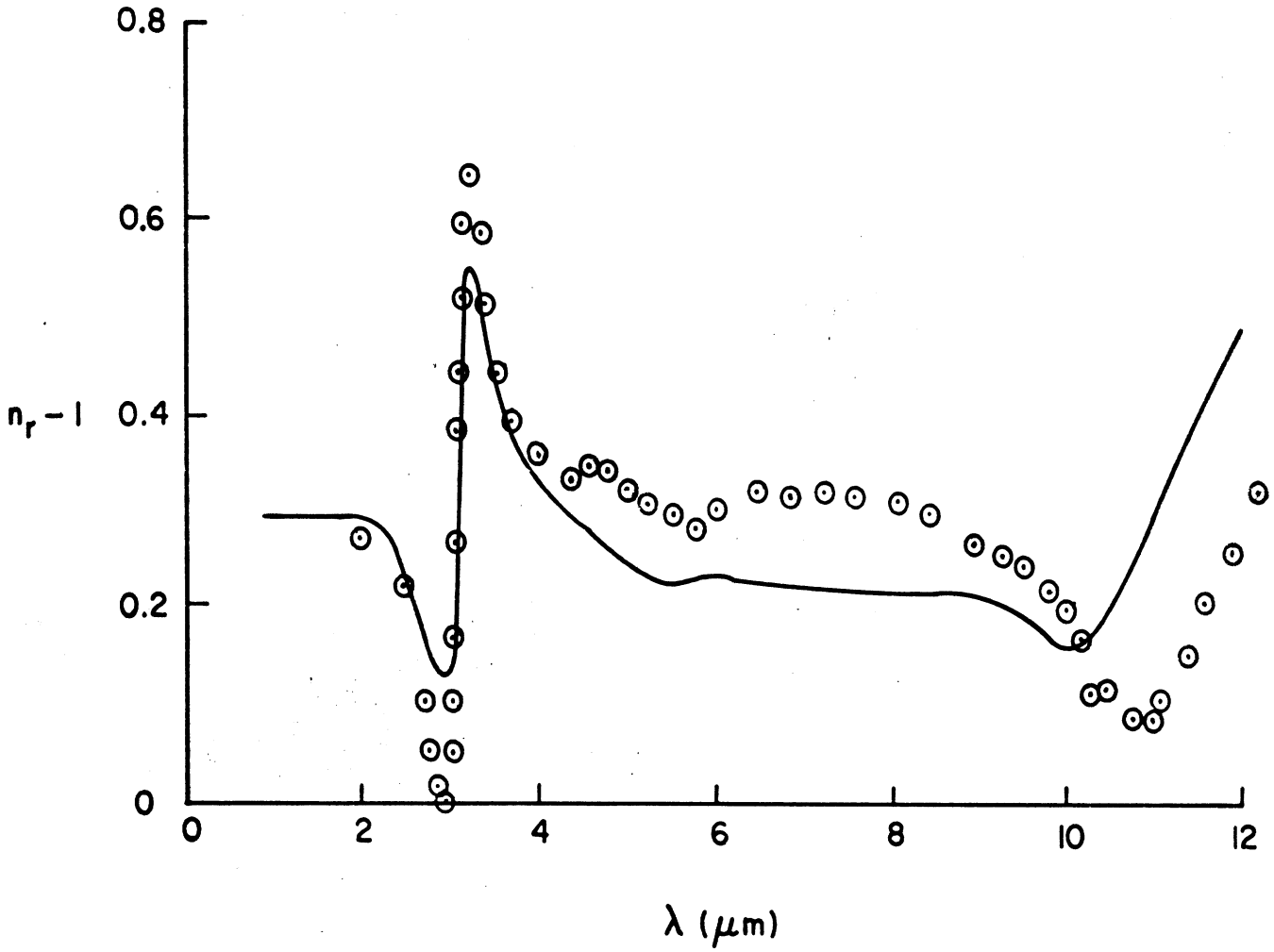


Figure 1a.

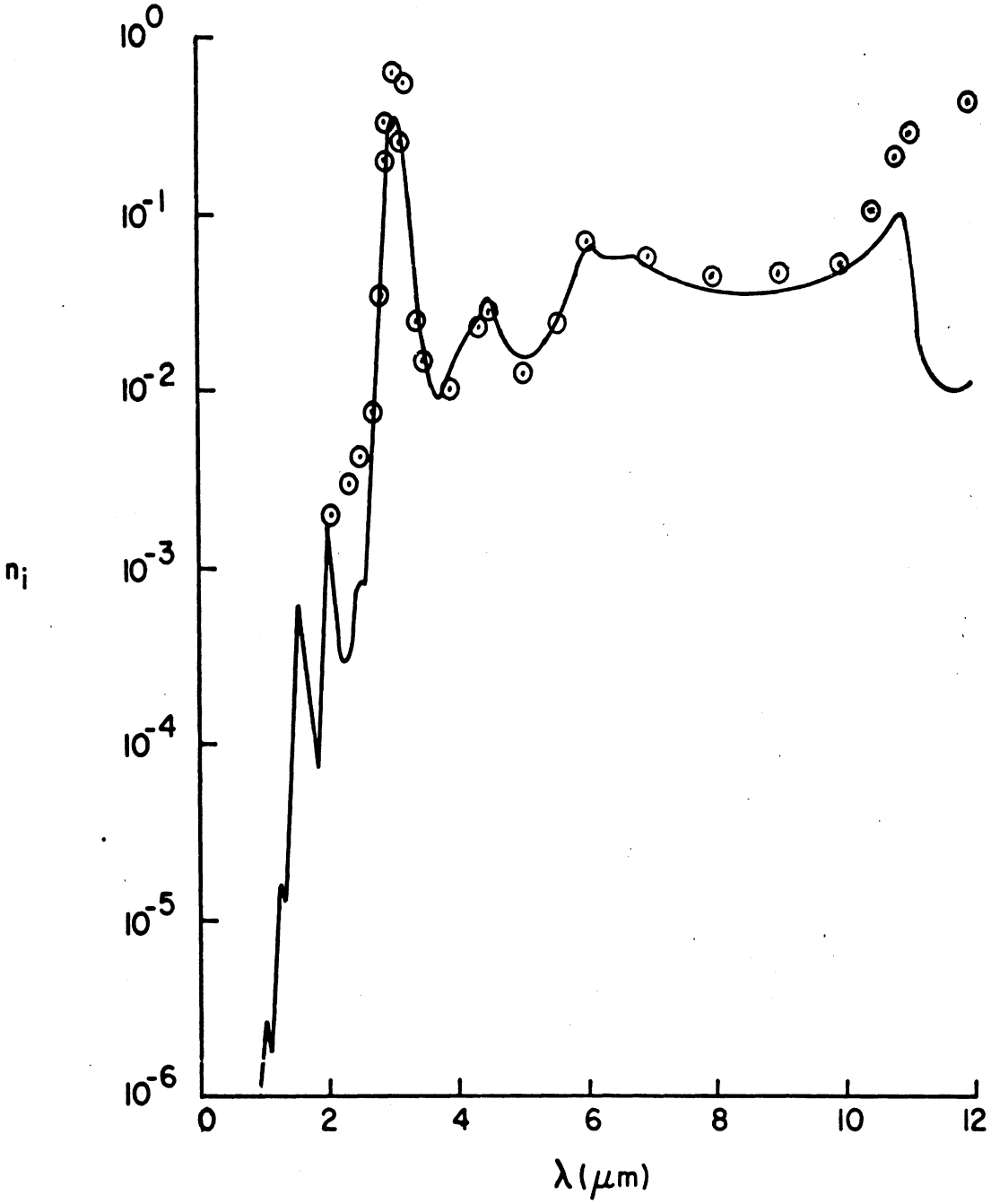


Figure 1b.

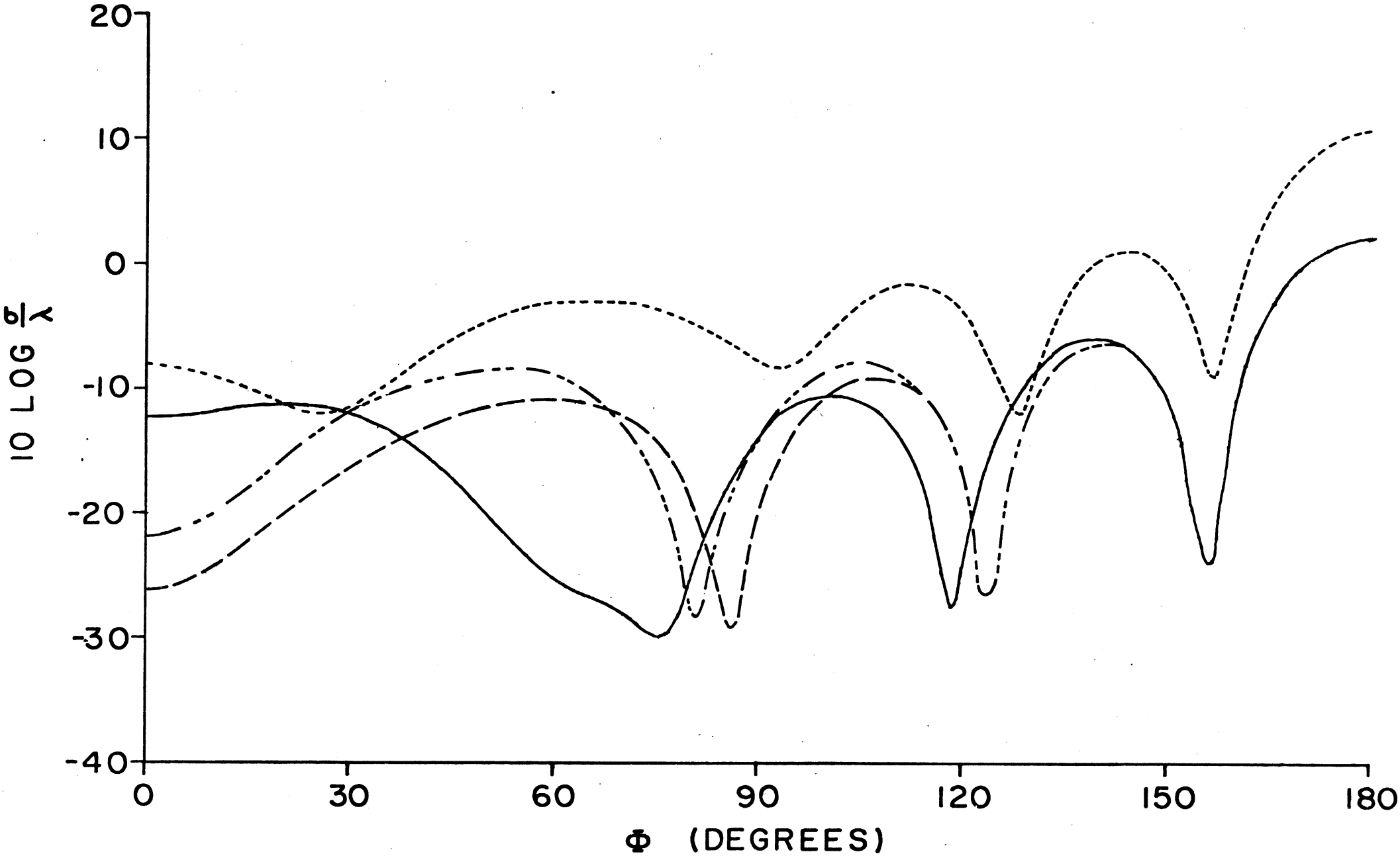


Figure 2a.

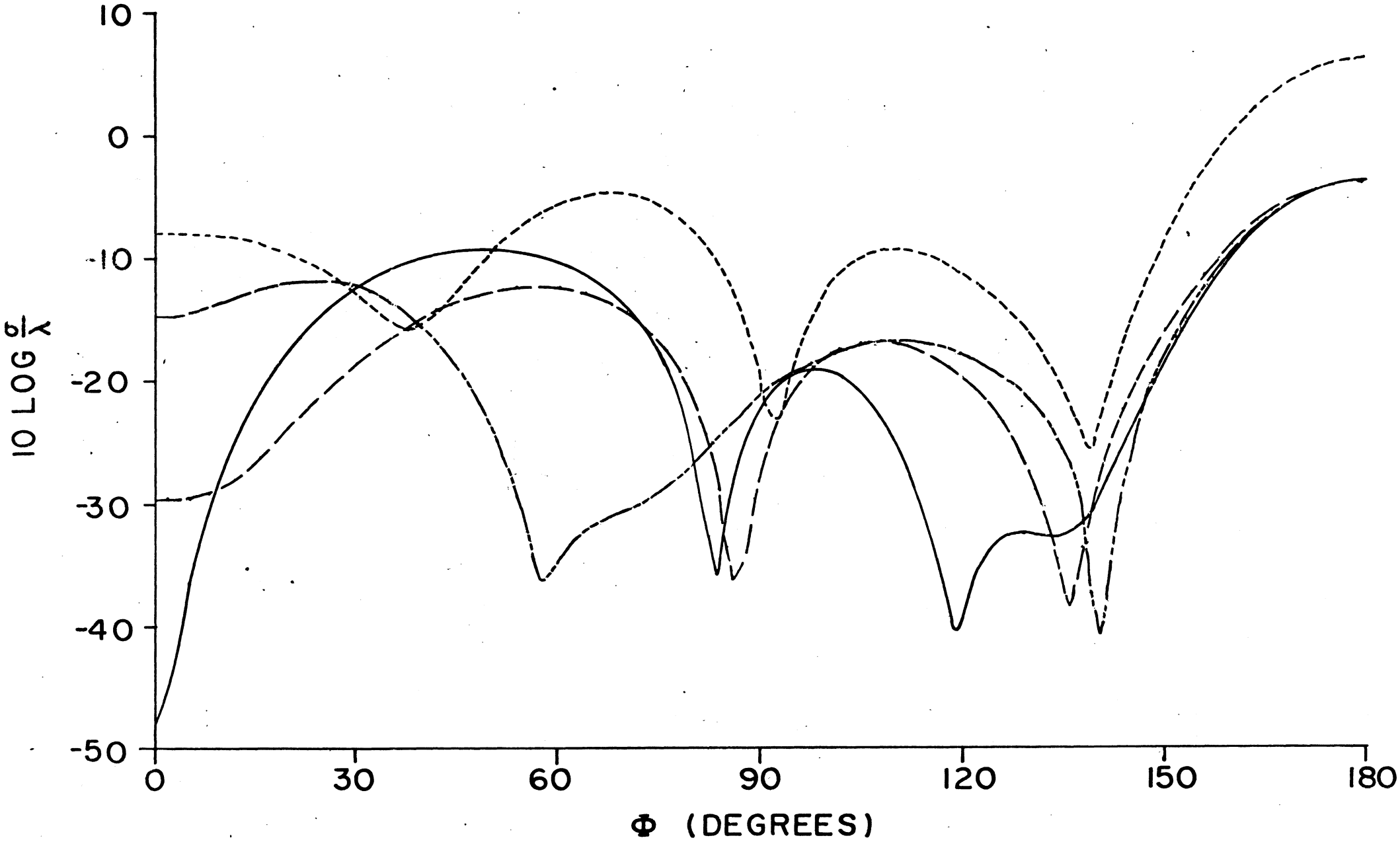


Figure 2b.

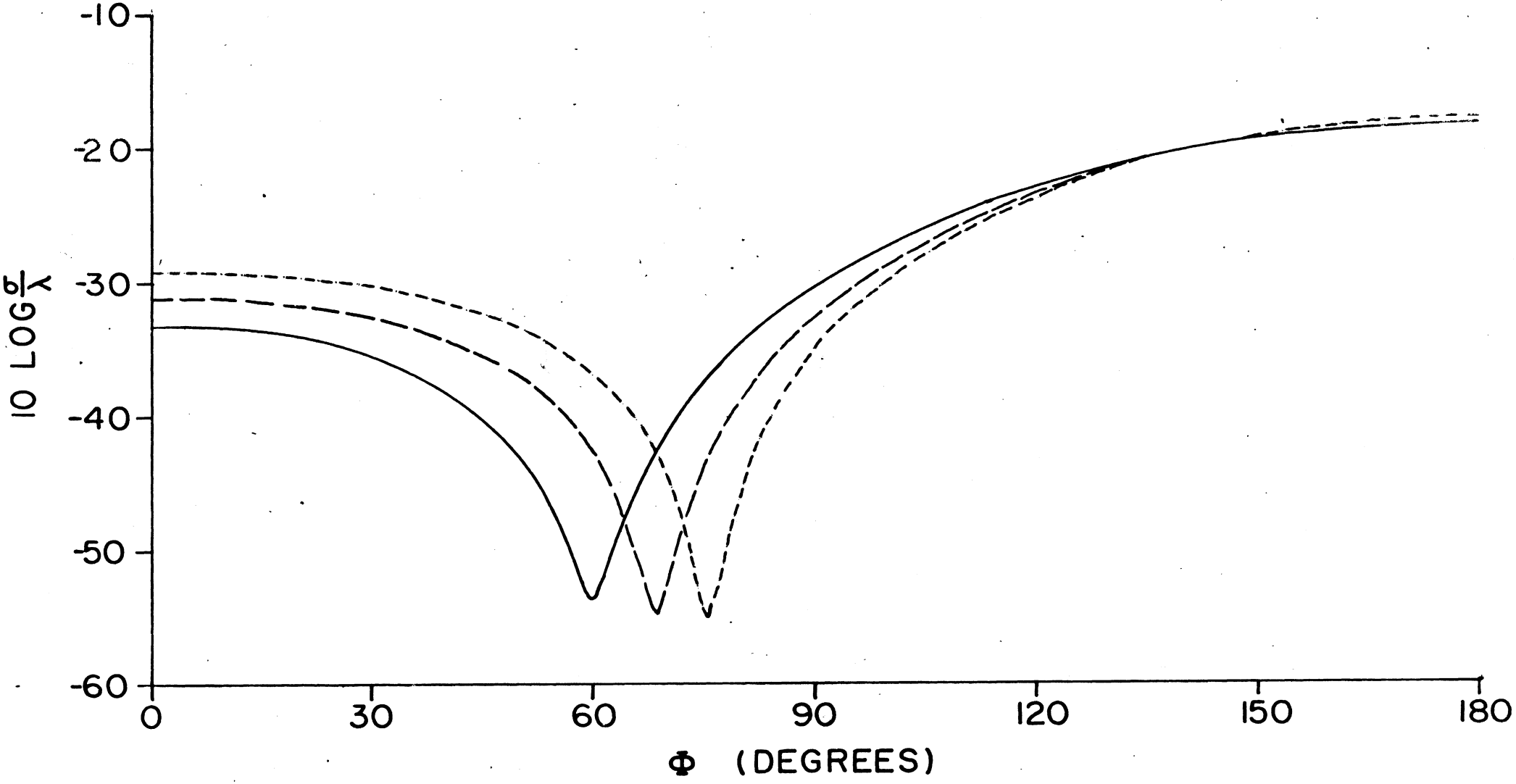


Figure 2c.

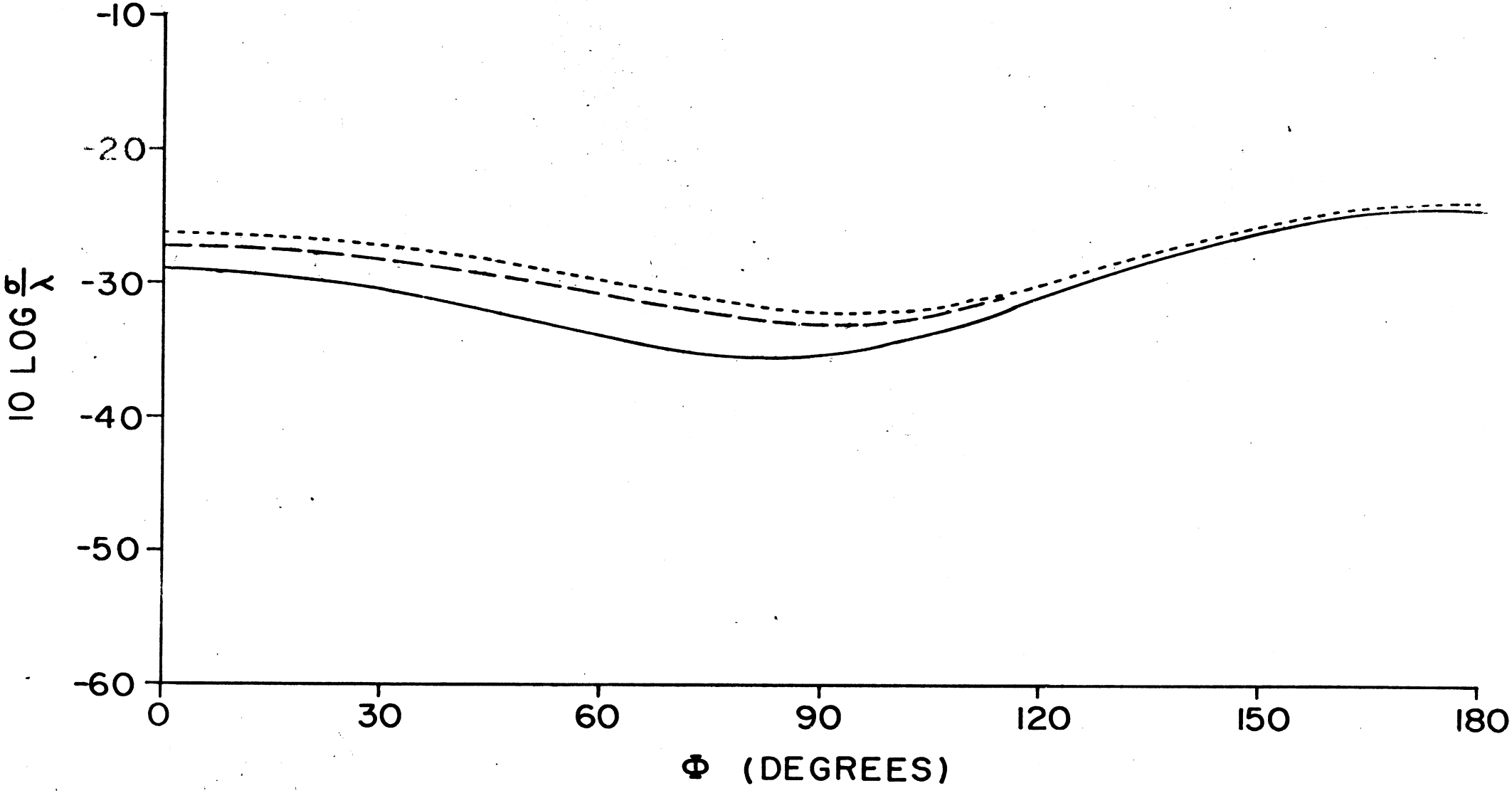


Figure 2 d.

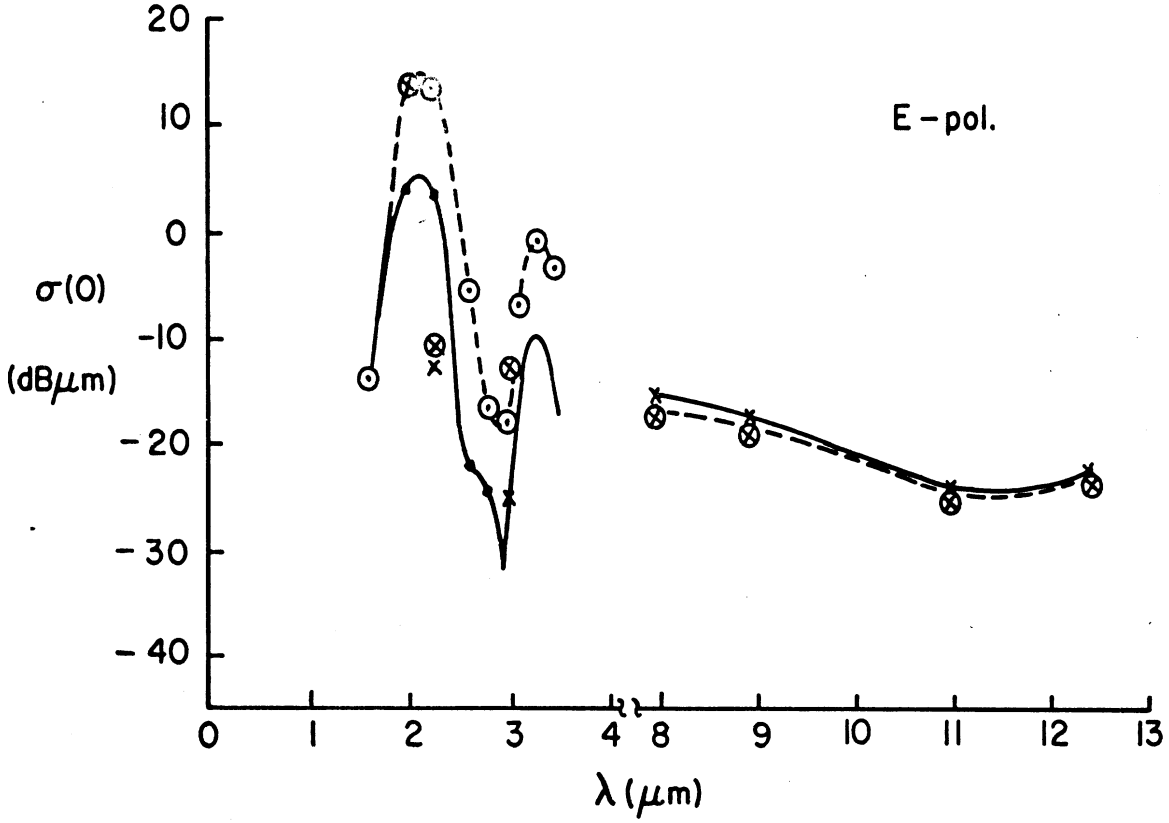


Figure 3a.

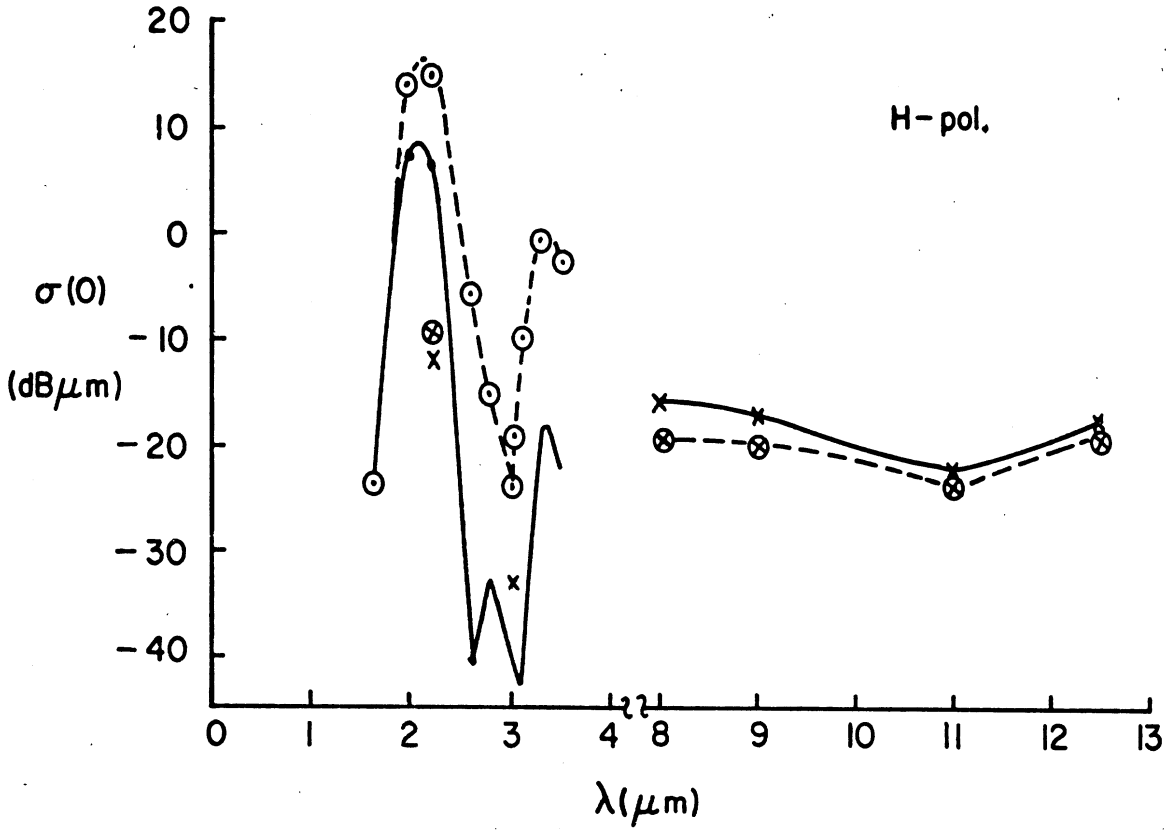


Figure 3b.

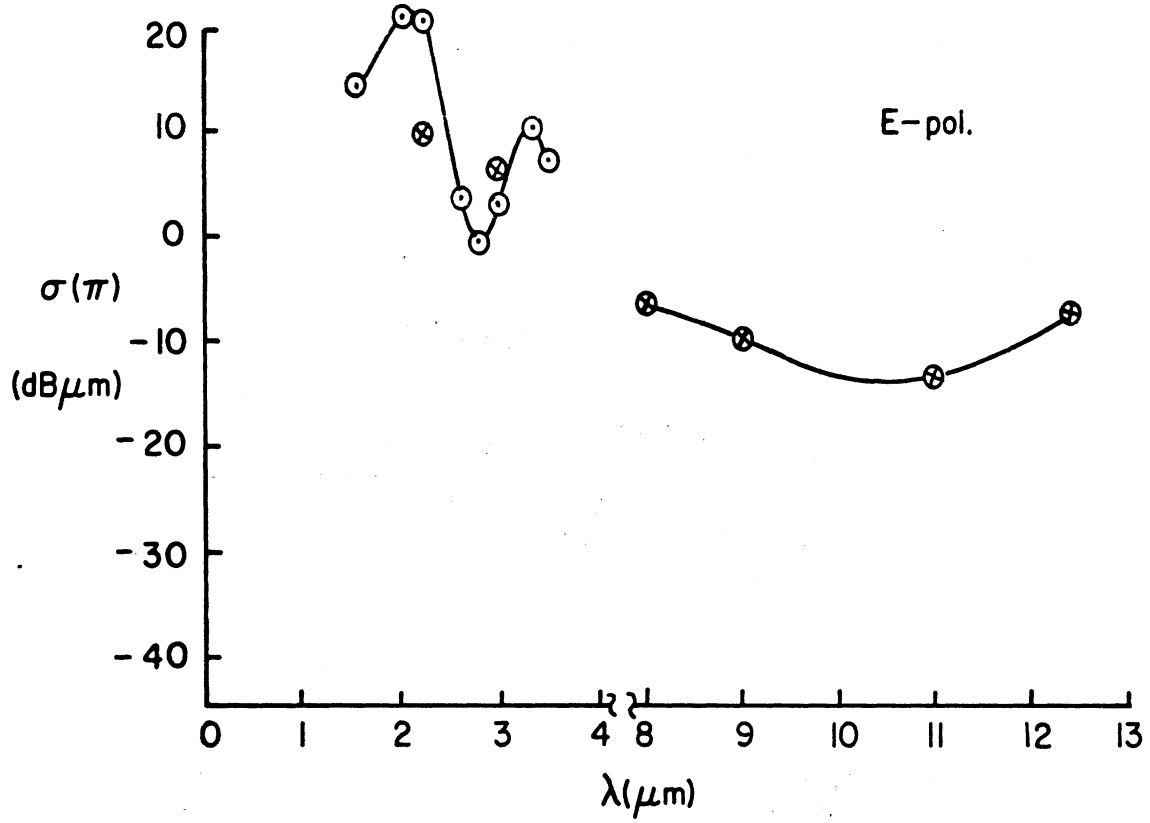


Figure 3 c.

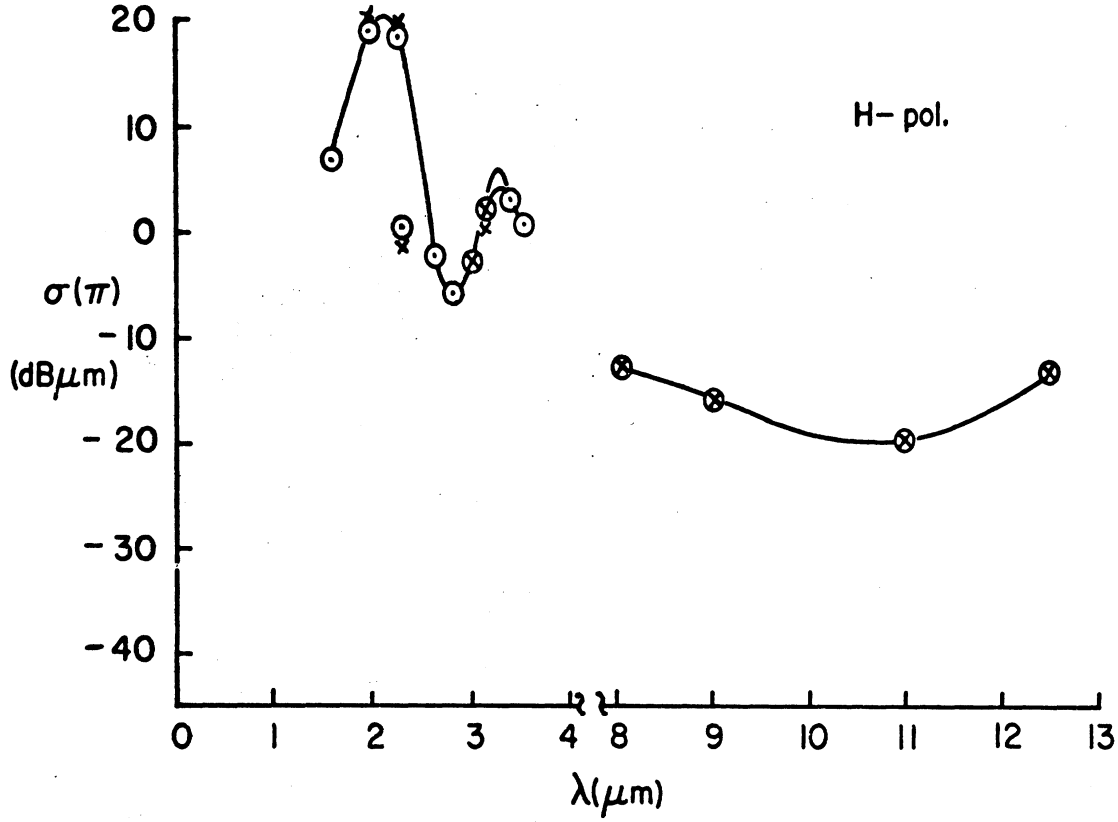


Figure 3 d.

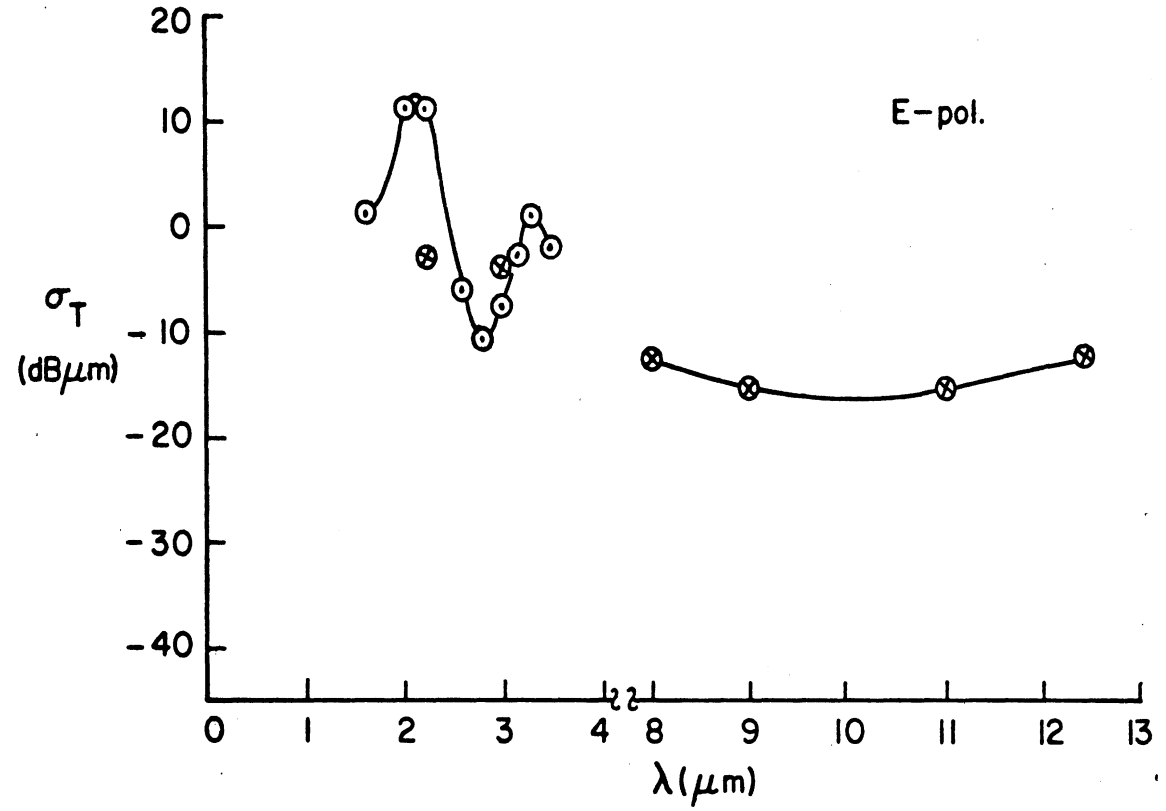


Figure 4a.

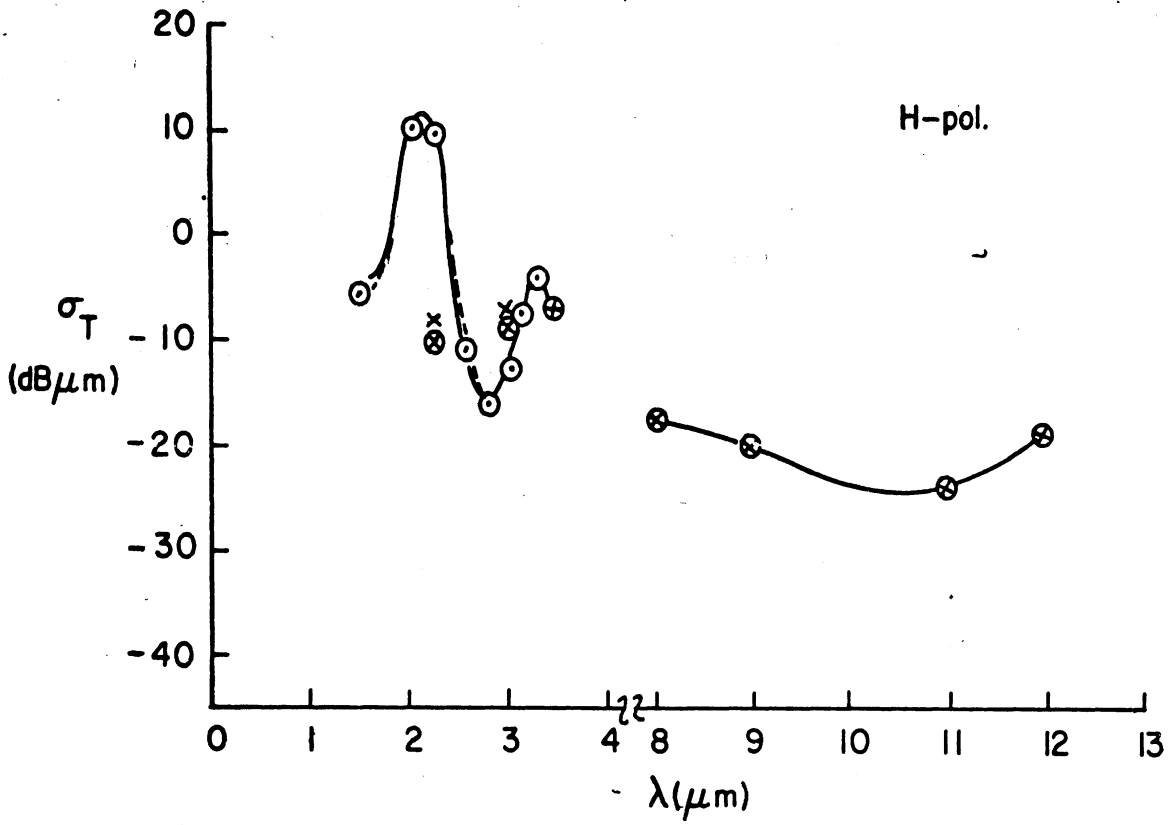


Figure 4b.

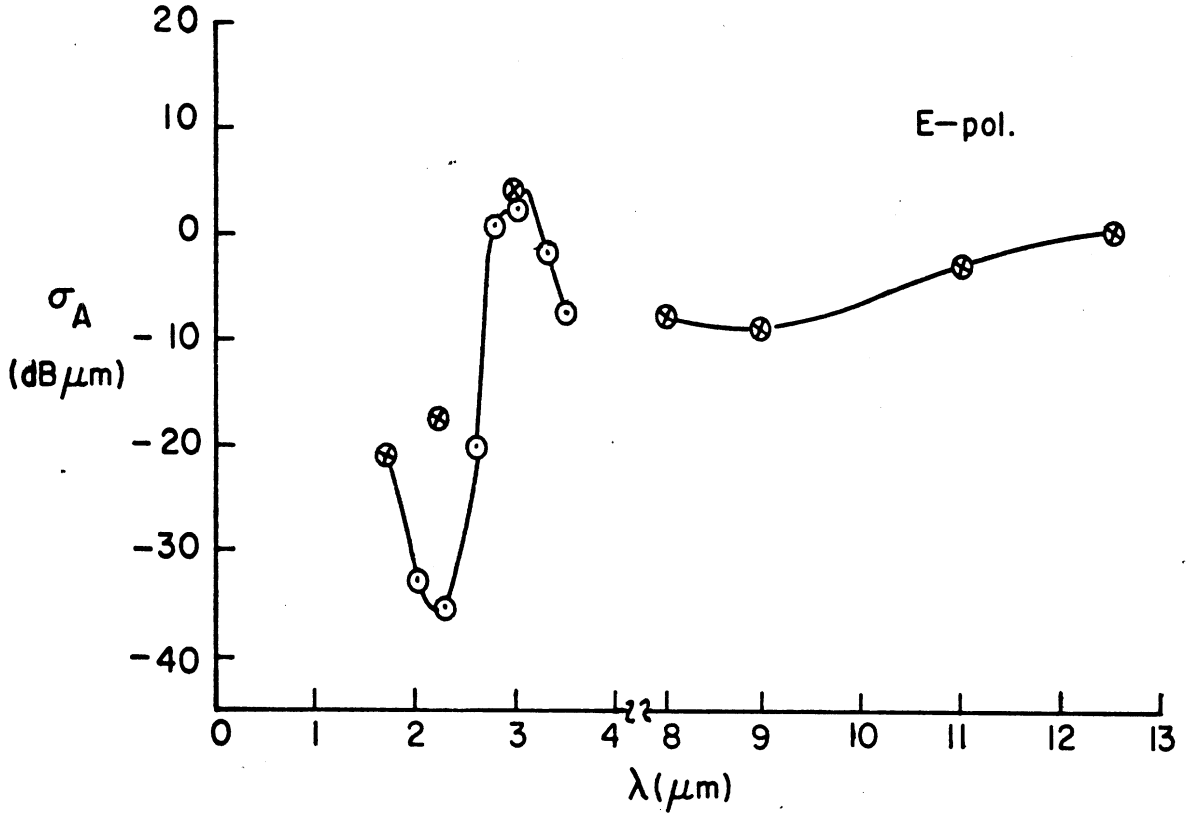


Figure 4c.

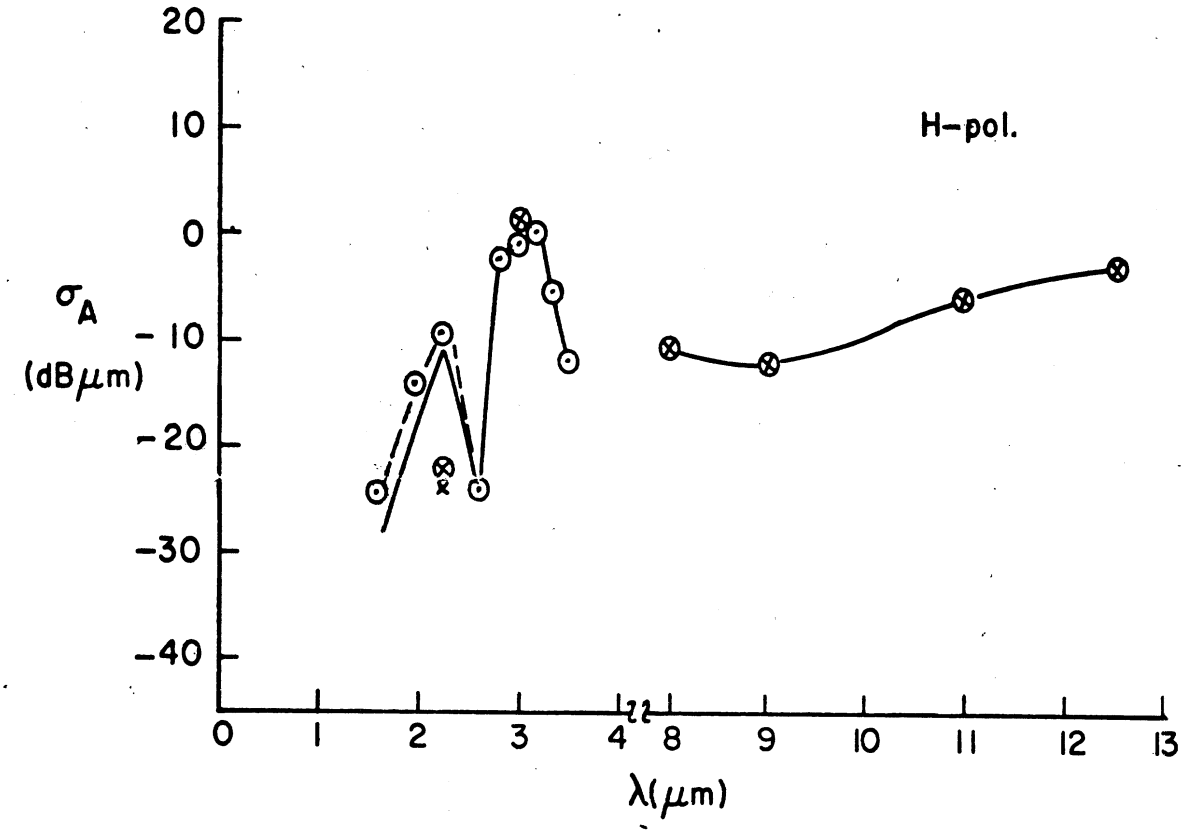


Figure 4d.